Analysis and Design of On-chip Spiral Inductors and Transformers for GaAs RF Integrated Circuits

A

Thesis submitted to

Indian Institute of Technology Kanpur
In partial fulfilment of the requirements for
The Degree of Master of Technology in
Electrical Engineering

Under the supervision of

Prof. Animesh Biswas

IIT Kanpur

&

Prof. Dr.-Ing. G. Böck

Institut für Hochfrequenz- und Halbleiter- Systemtechnologien ,TU Berlin

By

Akhilesh Mohan

Department of Electrical Engineering
Indian Institute of Technology Kanpur
July 2004

CERTIFICATE

It is certified that the work contained in the thesis entitled, *"Analysis and Design of On-chip Spiral Inductors and Transformers for GaAs RF Integrated Circuits"*, by *Akhilesh Mohan*, has been carried out under my supervision and that work has not been submitted elsewhere for a degree.

8 July,2004

Dr. ANIMESH BISWAS
Professor,
Department of Electrical Engineering
I.I.T. Kanpur

Acknowledgements

I would like to express my gratitude to all those who gave me the possibility to complete this masters thesis.

On the one hand, I want to thank Prof. Dr.-Ing. Georg Boeck, head of the Microwave Engineering Group of the Technical University of Berlin, for giving me permission to do this thesis in his group, for his support and his valuable hints.

On the other hand, I am deeply indebted to my supervisor Prof. Animesh Biswas whose help, stimulating suggestions and encouragement helped me all the time of research.

I extend my sincere thank to Dip.-Ing. Vasyl Dykyy for his assistance, suggestions for the writing of this thesis.

My colleagues from the Microwave Engineering Group at Berlin and Advanced Centre for Electronic System at Kanpur supported me too in my work. I want to thank them for all their help, support, interest and valuable hints.

I would like to take this opportunity to thank my parents whose encouragement helped me reach at this stage of my studies.

Table of Contents

List of Figures

Figures

List of Tables

Chapter 1

Introduction

1.1 Motivation

Today monolithic inductors and transformers are used extensively in different types of integrated radio frequency circuits. In earlier days they were realized as discrete components. But with the increasing demands on the application side more and more monolithic integrated inductors and transformers have been used for circuit design. This technique allows a realization of compact high frequency circuits with a high level of integration and low production costs.

Some typical applications of integrated inductors and transformers include for example:

- Input and output matching networks for amplifiers
- BALUN function in differential applications
- Mixers

At present it is possible to integrate lumped planar transformers in Si- and GaAs-based IC technologies which have acceptable performance characteristics in the 1-20 GHz frequency range. The outer dimensions are in the range of about 500 μm

down to 60 μm diameter depending on the frequency of operation and the IC technology.

The complete electrical characteristic of monolithic transformers and inductors cannot be predicted by closed form equations for complex structures. Numerical methods must be used to analyse it. There exist many commercially available electromagnetic field solvers which compute the field distribution of metal structures based on the Maxwell equations. The disadvantage of such 3-D numerical solver is that a full field calculation takes a too long computation time. Therefore it is not possible to optimize inductors or transformers by varying geometrical data of the structure in a reasonable amount of time. Another drawback is the limitation that many solvers only deliver the scattering parameters at the input and output ports. The scattering parameters cannot be used directly in a time domain or for large signal frequency domain circuit simulators (Harmonic Balance) along with other active and passive, linear and nonlinear RF circuit elements. For those reasons it is convenient to develop different calculation methods to predict the electrical characteristics and to provide an equivalent model.

Our motivation for this research is to fill the gap and have a program which models inductors and transformers accurately and gives quick results, which are close to the measured values.

1.2 Thesis Overview

Chapter 2 gives an overview on characterization of inductors and transformers. Basic electromagnetic effects are illustrated. Lumped low order models and an extension to generate higher order models are introduced using the low order models for inductors and transformers.

Chapter 3 describes the parameter extraction method from the physical structure. The parameter extraction includes the inductance, substrate capacitance, serial resistance, inter-winding capacitance, crossing area capacitance and coupling factor.

Chapter 4 shows the measurement set-up and gives description about the simulated and measured results of the inductor and the transformer.

Chapter 5 describes a typical application of transformer in a mixer in RF integrated circuit design.

Chapter 6 discuss about the high performance inductors which shows in which configuration inductors have maximum quality factor..

Concluding remarks and the future works are presented in Chapter 7.

Chapter2

Modeling

In this chapter equivalent models of planar inductors and transformers are derived from the physical layout. The treatment starts with short overview of the physical effects. Afterwards appropriate equivalent electrical models are introduced.

2.1 Physical Layout

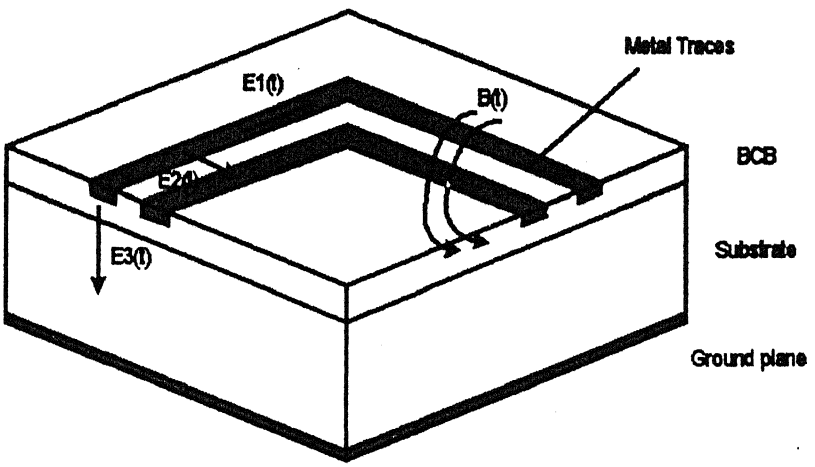

Figure 2.1 Schematic cross-section of a planar inductor.

Monolithic transformers and inductors are constructed using conductors inter-wound in the same plane or overlaid on multiple stacked layers. They can be implemented in circular or rectangular shape with different winding configurations. Each of these realizations shows specific performance advantages. There exists many publications which describe these possibilities in construction and optimization of inductors and transformers.

Independent on their geometrical structures there affects always the same physical phenomenon on the structures. Figure 2.1 shows a schematic cross-section of a planar inductor. It gives an insight into the basic physical effects. The pictures shows only two adjacent turns realized on one metal layer embedded in BCB layer. The conductors are separated from the substrate by BCB layer. This simplified model is sufficient to illustrate the different electromagnetic fields that are present in an inductor when excited.

Around the traces exists a time varying magnetic field B(t), created by the current flow in the metal. B(t) is responsible for the stored magnetic energy and the resulting inductance. Further, in the case of transformers B(t) is responsible for coupling between the primary and secondary winding.

Unfortunately there are also exists other electromagnetic field that decrease the performance of inductors and transformers which result in losses produced due to the non ideal physical properties of the used materials. Each of the electric field components E1-E3 in fig results in the loss of energy in the whole structure. E1(t) is the electric field along the metal trace. It is caused by the current in the winding and the finite conductivity. The current causes in association with ohmic losses a voltage drop

an electric field denoted by E2(t) . Due to the finite resistance and capacitive coupling a leakage current flows from turn to turn. In the similar manner the electric field component E3(t) forces a leakage current between the metal traces and ground.

In addition to the described electromagnetic fields, many other high-order effects are present. For instance, eddy currents arise in the metal traces and force a skin effect due to penetration of time varying magnetic fields. Further a proximity effect occurs due to the interaction between the magnetic field and currents. Both results in increased resistances and losses. Additionally currents induced in the substrate give rise to counterproductive secondary magnetic fields which interact with the primary magnetic field B(t).

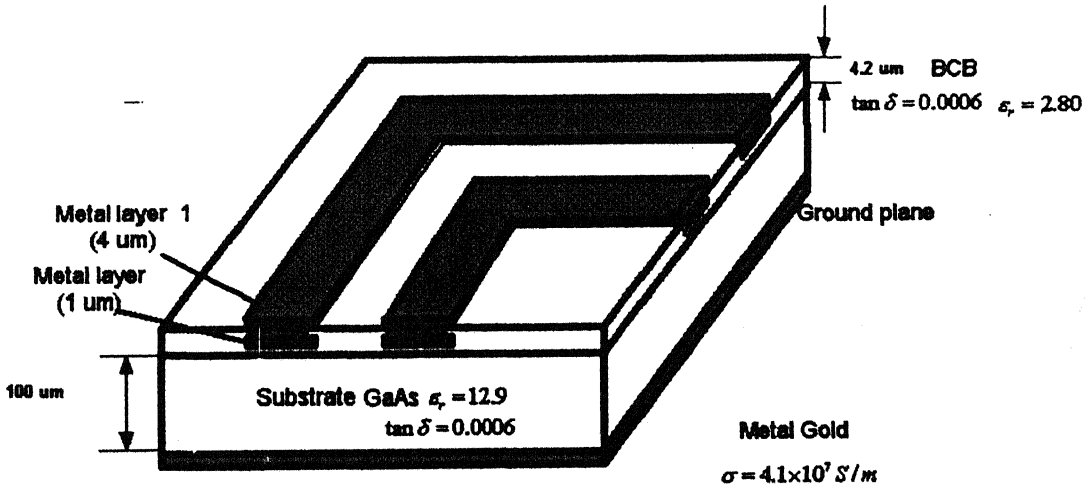

Figure 2.2 Properties of substrate GaAs, BCB and metal used

Low-resistance metal interconnects and low-k dielectric materials such as BCB (benzocyclobutene) we have used in GaAs IC manufacturing to reduce the losses. The GaAs devices have been fabricated using lower resistance gold interconnects. Since

GaAs devices have been fabricated using lower resistance gold interconnects. Since GaAs is a semi-insulating material resistivity of the order of 10^9 Ωm, so we nave neglect the substrate resistance in parallel with the substrate capacitance.

2.2 Physical Model

An alternative to a fully 3-D field analysis is an approximation with electrical lumped elements (R, L, C). This is valid because the physical lengths of the conducting segments in the layout are typically much less than guided wavelength at the frequency of operation. The analysis is reduced to electrostatic and magnetostatic calculations for easier treatment in order to this approximation.[1]

In the physical model each circuit is related directly to the physical layout. This property is very important when designing new inductors or transformers where measurements data are not available.

The key to accurate physical modelling in this way is the ability to describe the behaviour of the inductance and the parasitic effects. Each lumped element of the model should be consistent with the physical phenomena occurring in the part of structure it represents. In a pure physical model the value of electrical lumped elements is only determined by the geometry and material constants of the structure.[2-3]

At modelling we have to make decision about the accuracy and limitations of the model. The integration of several lumped elements gives only an estimation of the electrical behaviour. It is clear that the number of elements determines the grade of the approximation. With increasing the number of elements the precision increases. On the

other hand the simulation time rises too. A compromise between accuracy and simulation time has to be done.

2.3 Low-Order Inductor Model

The aim of low order models is to reduce the number of parts in the equivalent circuit to a minimum. The following proposed low-order model allows a characterization of the inductor up to its first self resonance frequency. Near and above the self resonant frequency the model fails due to the low-order.

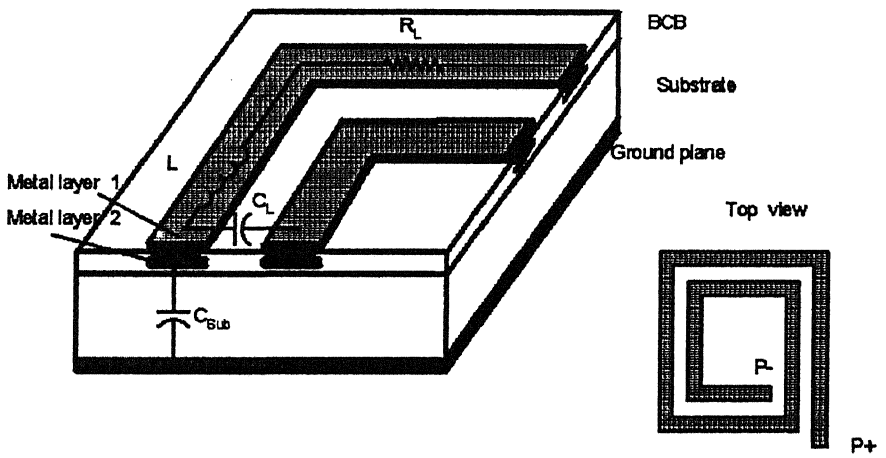

Figure 2.3 Three dimensional cross-section of a monolithic inductor.

The basic idea is to model whole winding as one lumped element with two ports. Accordingly, the inductance and all parasitics just relate to one physical element, which parasitics appear and how they have to be arranged in an equivalent electrical circuit can be easily found in figure 2.3. The cross-section of a rectangular inductor realized on two metal layers is shown.

The lumped elements can be identified as:

The lumped elements can be identified as:

- L, Inductance due the magnetic flux.
- R_L, Ohmic loss in the conductor material due to skin effect, current crowding and finite conductivity.
- C_L, Parasitic capacitive coupling between the winding turns.
- C_{Sub}, Parasitic capacitive coupling into the substrate.

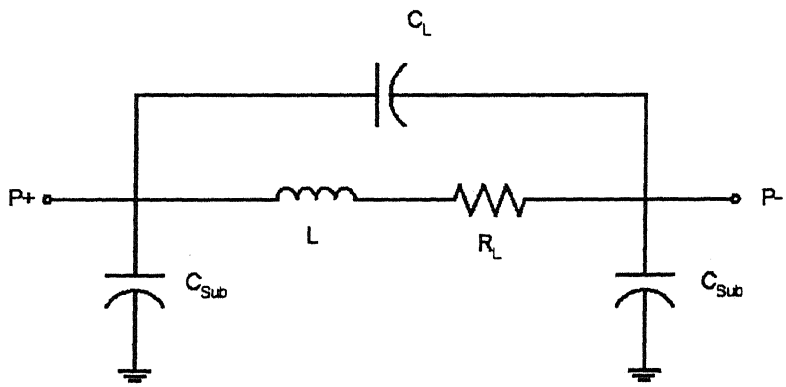

Figure 2.4 Low-order inductor model.

Figure 2.4 shows the resulting equivalent circuit. It represents a symmetrical pi-circuit with ports on both sides. The series branch consists of the overall inductance L and serial resistance R_L which appears along the whole winding. C_L is located between the terminals and represents the losses due to the capacitive coupling from winding to winding.

Note, that the capacitance C_L models the parasitic capacitive coupling between the input and output port of the inductor. The capacitive coupling between is based on the crosstalk between the adjacent turns. The capacitance allows the signal to flow

directly from the input to the output port without passing through the inductor. Since the crosstalk effect depends on the potential difference between the turns it is not trivial to determine the equivalent capacitor C_L between the ports. For modelling this capacitor it is necessary to take the voltage profile along the winding into account.

All other parameters can be static investigations of the inductor structure.

2.4 Higher-Order Inductor Model

The use of additional circuits elements results in more accuracy in characterization of the physical structure. This can be achieved by creating higher-order models. Compared to the low order model the lumped elements are not derived from the impact of the whole winding. Furthermore the structure is sectioned into multiple individual segments. Each of them will be characterized by an equivalent sub-circuit.[4] The electrical behaviour of the whole inductor yields by joining the sub-circuits related to the physical structure. In a first approximation the inductor winding can be divided into straight conductor elements.

Figure 2.5 shows such a rectangular spiral inductor divided into 8 segments. The physical layout is partitioned into several coupled straight conductor lines. Each line has a similar pi-equivalent circuit as the inductor shown earlier except the capacitor C_L

These lumped pi-elements are then joined serially to model the entire inductor structure. Also the capacitive and inductive coupling between the segments must be taken into account and considered as a capacitance between each segment and as coupling factor between each inductance. Fig.2.6 shows the resulting high-order model that results from physical structure. Note that the model just considers the capacitive

coupling between two adjacent parallel segments. This approximation is valid since the capacitive coupling to the other segments is very small.

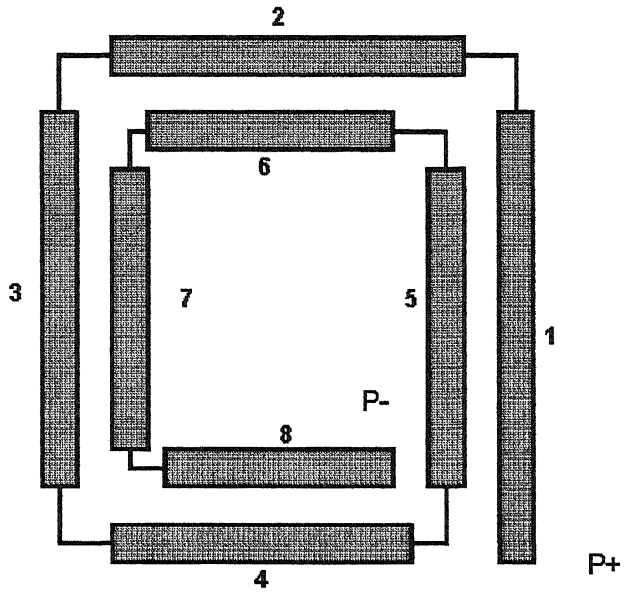

Figure 2.5 Segmentized rectangular spiral inductor.

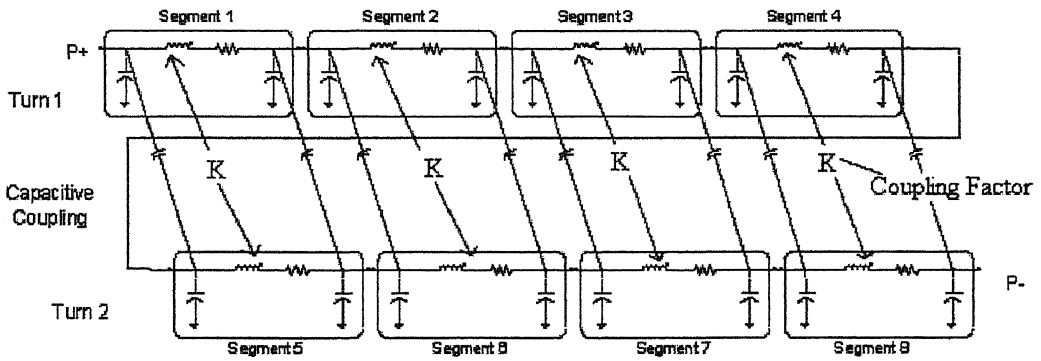

Figure 2.6 Inductor higher-order model.

2.5 Transformer Model

The operation of transformers is based upon the magnetic coupling between two windings. Each winding, primary and secondary has a self inductance L_P, and L_S. The magnetic coupling between the windings is expressed by the mutual-inductance M. In case of ideal transformer this information is sufficient to create an equivalent circuit.

Alternatively to the specification of the mutual inductance it is possible to a coupling coefficient *k*. It represents the strengths of coupling between the primary and secondary winding.

$$k = \frac{M}{\sqrt{L_P L_S}} \tag{2.1}$$

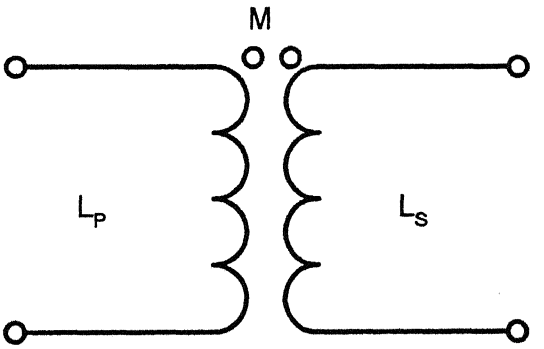

Figure 2.7 Ideal transformer equivalent circuit.

Generally, monolithic transformers are always afflicted with several loss mechanisms which originate in the use of non-ideal materials. Since the construction of the monolithic transformers consists of two planar inductor windings realized in the same manner as parasitic phenomena takes place. An equivalent low-order transformer circuit can be found based on the low-order inductor model.

Chapter 3

Parameter Extraction

A lumped low order model for inductors and transformers is found in last Chapter 2. This chapter describe the parameter extraction method from the physical structure.

In parameter extraction, we have to find how the parameters of the physical model depend upon the geometrical parameters of the physical model. To perform this task, first we have taken simple single metal strip on the substrate and analyse it with three software Agilent ADS[5], Ansoft HFSS[6] and Agilent Momentum[5]. The structure of the single line is shown below in the figure 3.1

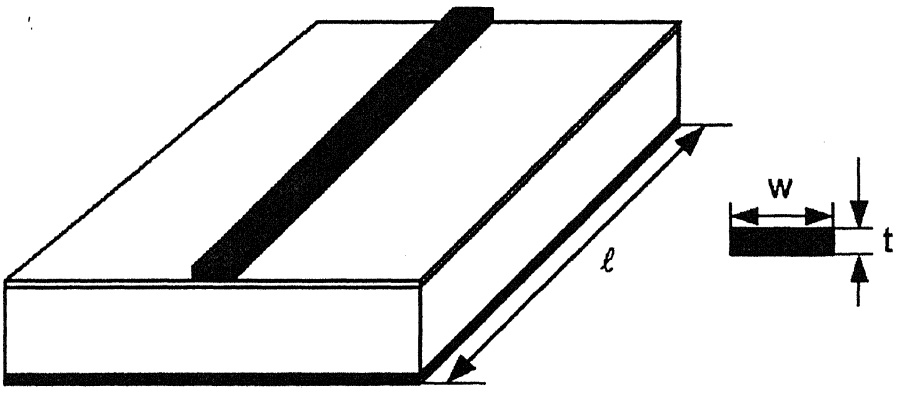

Figure 3.1 Structure of a single strip of the metal.

The values of inductance, capacitance and resistance are calculated by equalizing the scattering parameters of the modelled and the simulated structure. They are extracted for different lengths and widths by using different software.

As shown in figures 3.2, 3.3 and 3.4 we finally analyse that taking data from ADS will be better than the other two. By using ADS data in MATLAB[7] and using curve fitting and the parameters depend linearly on the length.

3.1 Inductance Calculations

Inductance calculation of metal structures is based on Maxwell equation.

$$\vec{\nabla} \times \vec{H} = \vec{J} + \frac{\partial \vec{D}}{\partial t} \tag{3.1}$$

With this equation it is possible to derive an inductance value for arbitrary 3-D structures[8-9]. Unfortunately in most cases it does not exist a closed form expression. Therefore numerical methods must be used to solve the problem in this way.

Table 3.1
Inductance of the single line for different widths

Width	Inductance (L) in nH
5 um	L=0.00089ℓ+0.015
10 um	L=0.00080ℓ+0.010
15 um	L=0.00073ℓ+0.008
20 um	L=0.00065ℓ+0.009

where ℓ is the length in um.

From the above equations we find that the coefficients of ℓ depends upon the width of the metal strip and the finally inductance depends out to be ℓ and w, both are in um

$$L = [(-1.6 \times 10^{-5})\, w + 0.00097]\, \ell + 0.01 \tag{3.2}$$

where L is in nH.

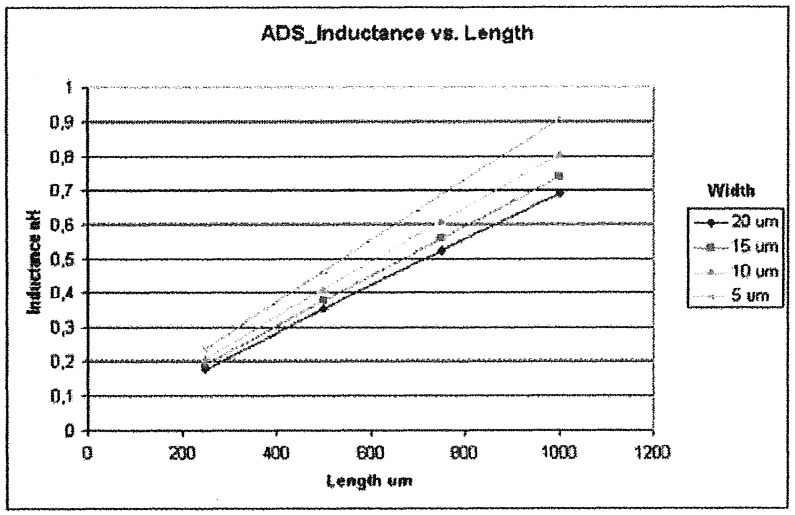

(a)

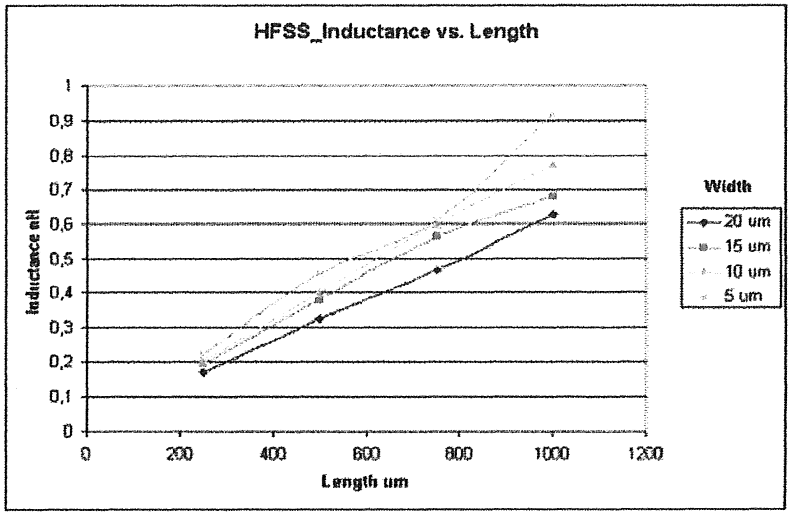

(b)

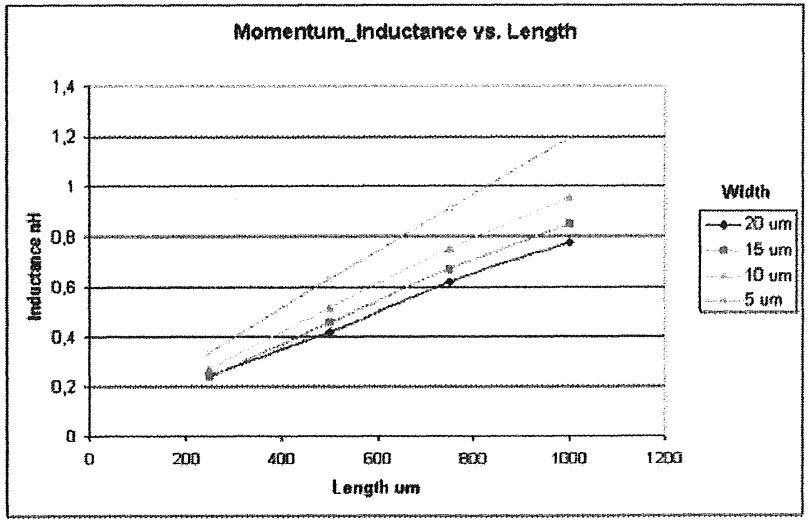

(c)

Figure 3.2 Inductance nH vs. Length um in (a) ADS (b) HFSS and (c) Momentum

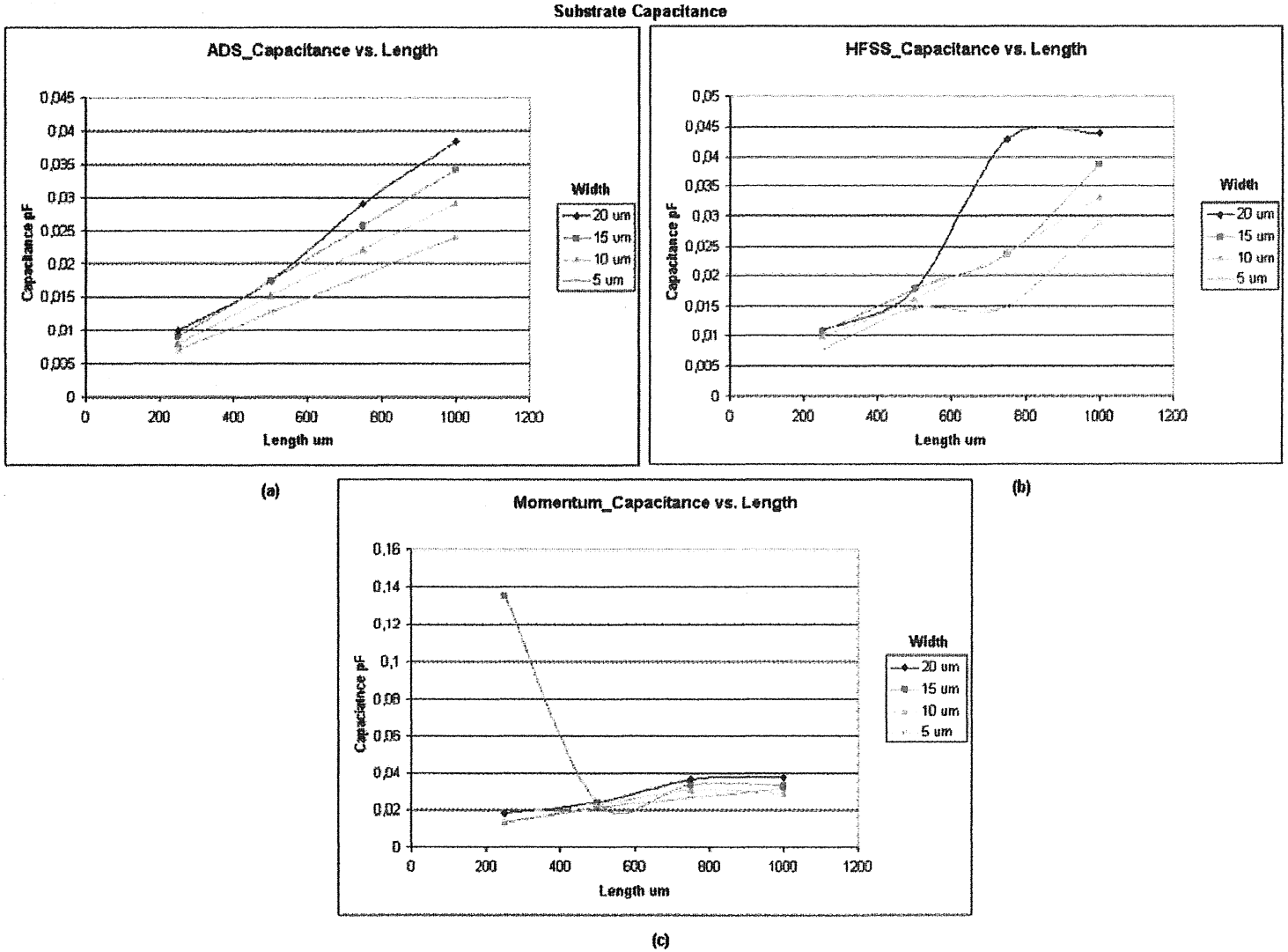

Figure 3.3 Capacitance pF vs. Length um in (a) ADS (b) HFSS and (c) Momentum

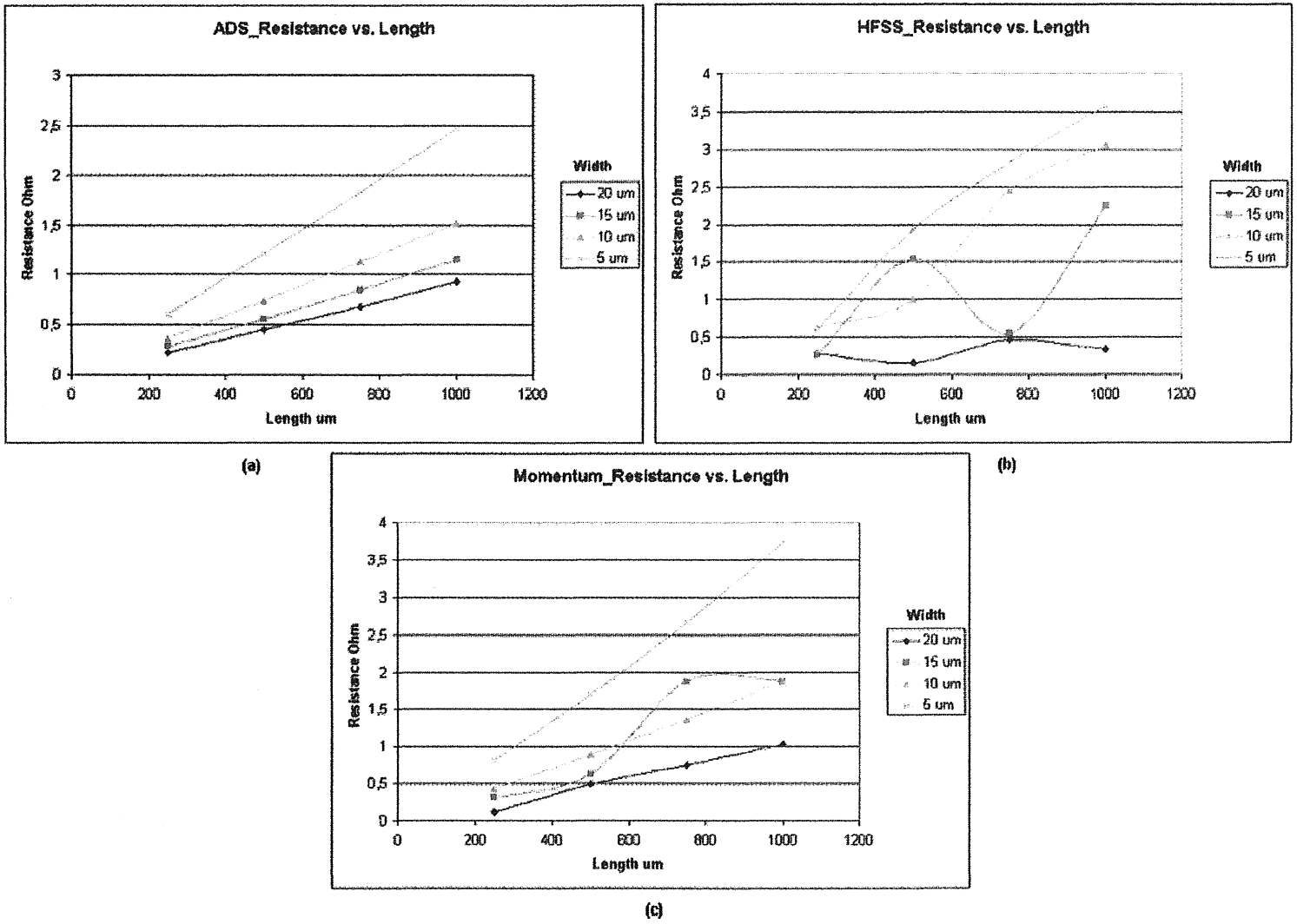

Figure 3.4 Resistance Ohm vs. Length um in (a) ADS (b) HFSS and (c) Momentum

3.2 Substrate Capacitance Calculations

The Substrate capacitance is given for different widths are as follows

Table 3.2
Capacitance of the single line for different widths

Width	Capacitance (C) in pF
5 um	$C=2.3 \times 10^{-5}\ell+0.0014$
10 um	$C=2.8 \times 10^{-5}\ell+0.0011$
15 um	$C=3.4 \times 10^{-5}\ell+0.0006$
20 um	$C=2.8 \times 10^{-5}\ell+0.0007$

where ℓ is the length in um.

From the above equations we find that the coefficients of ℓ depends upon the width of the metal strip and the finally capacitance depends out to be ℓ and w , both are in um.

$$C = [(0.1w+1.81) \times 10^{-5}]\ \ell+0.001 \qquad (3.3)$$

where C is in pF.

3.3 Serial Resistance Calculations

The serial resistance is given for different widths are as follows

Table 3.3
Resistance of the single line for different widths

Width	Resistance in Ohm
5 um	$R=0.0025\ell-0.030$
10 um	$R=0.0015\ell-0.022$
15 um	$R=0.0012\ell-0.017$
20 um	$R=0.00093\ell-0.014$

where ℓ is the length in um.

From the above equations we find that the coefficients of ℓ depends upon the width of the metal strip and the finally resistance depends out to be ℓ and w , both are in um , and we neglect the constant term which is small as compared to

$$R = 1.5 \times 10^{-8} (\ell/w) \tag{3.4}$$

where R is in Ohm.

The ohmic losses in the winding are caused by finite conductivity of the metal. An analytical estimation of series resistance may be obtained from the basic formula of straight conductors:

$$R = \rho \frac{l}{wh} \tag{3.5}$$

where ρ represents the resistivity of the material in ohm m , l is the length of the winding in m and w, h are the cross-section dimensions of the winding trace in m. We have used this formula rather than above calculated one.

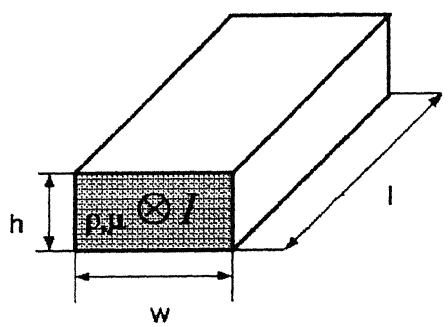

Figure 3.5 Straight rectangular conductor.

The above equation is valid for a uniform current distribution along the cross-section. This condition is fulfilled only for direct current and low frequencies. At increasing frequencies the current density becomes more and more non-uniform due high frequency effects in the metal. They can be identified as skin effect. The origin of it lies in penetration of time varying magnetic fields in the metal.

At the skin effect the magnetic field in the metal is produced by the current flow in the conductor itself. The induced eddy currents in the conductor force most of the current to flow near the boundary of the metal conductor. In consequence of the higher current density on the edges, the serial resistance in the rectangular conductors based on the direct current case was given by Lofti.[11]

$$R_{AC} = R_{DC}\left[1+\left(\frac{f}{f_l}\right)^2+\left(\frac{f}{f_u}\right)^5\right]^{\frac{1}{10}} \tag{3.7}$$

$$f_l = \frac{\pi\rho}{2\mu wh}\,,\; f_u = \frac{\pi^2\rho}{\mu h^2}\left[K\left(\sqrt{1-\frac{h^2}{w^2}}\right)\right]^{-2} \tag{3.8}$$

where w, h are the cross-section dimensions in m, μ is the permeability of the metal. R_{DC} is the resistance in the direct current mode. The frequencies f_l and f_u are the cutting frequency of the low frequency case and of the high frequency case. K is the complete elliptical integral of first kind:

$$K(x) = \int_0^{\frac{\pi}{2}} \frac{1}{\sqrt{1-x\sin^2\phi}}\,d\phi \tag{3.9}$$

3.4 Coupling Factor

We have calculated the inductance, capacitance and resistance of single line. Now further we have to calculate the mutual inductance or coupling factor and the inter-winding capacitance using parallel coupled lines. The structure of the parallel coupled lines is shown in the figure 3.6

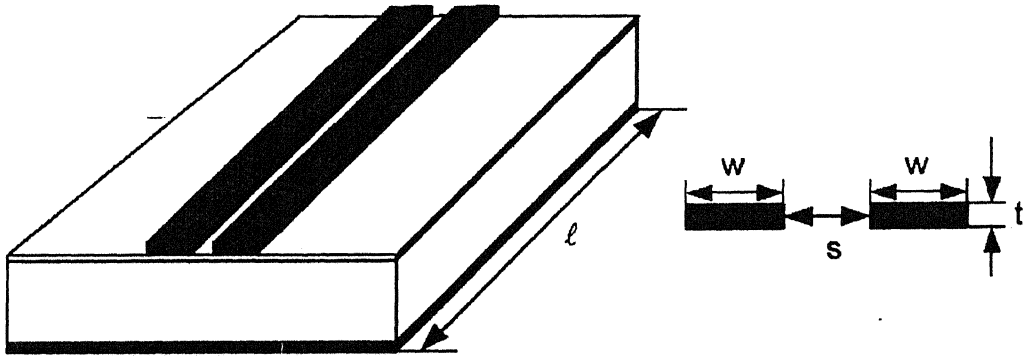

Figure 3.6 Structure of a parallel coupled lines

For calculating the coupling factor and inter-winding capacitance we have used the above calculated inductance, substrate capacitance and resistance and by comparing the scattering parameters of the modelled and ADS structure we are able to find it.

From the figure 3.7 we assume that the coupling factor varies as

$$K=A+B\exp(-Cs) \qquad (3.10)$$

where A, B and C are functions which depends on the length and width of the strip and s is the spacing between the metal strip in um.

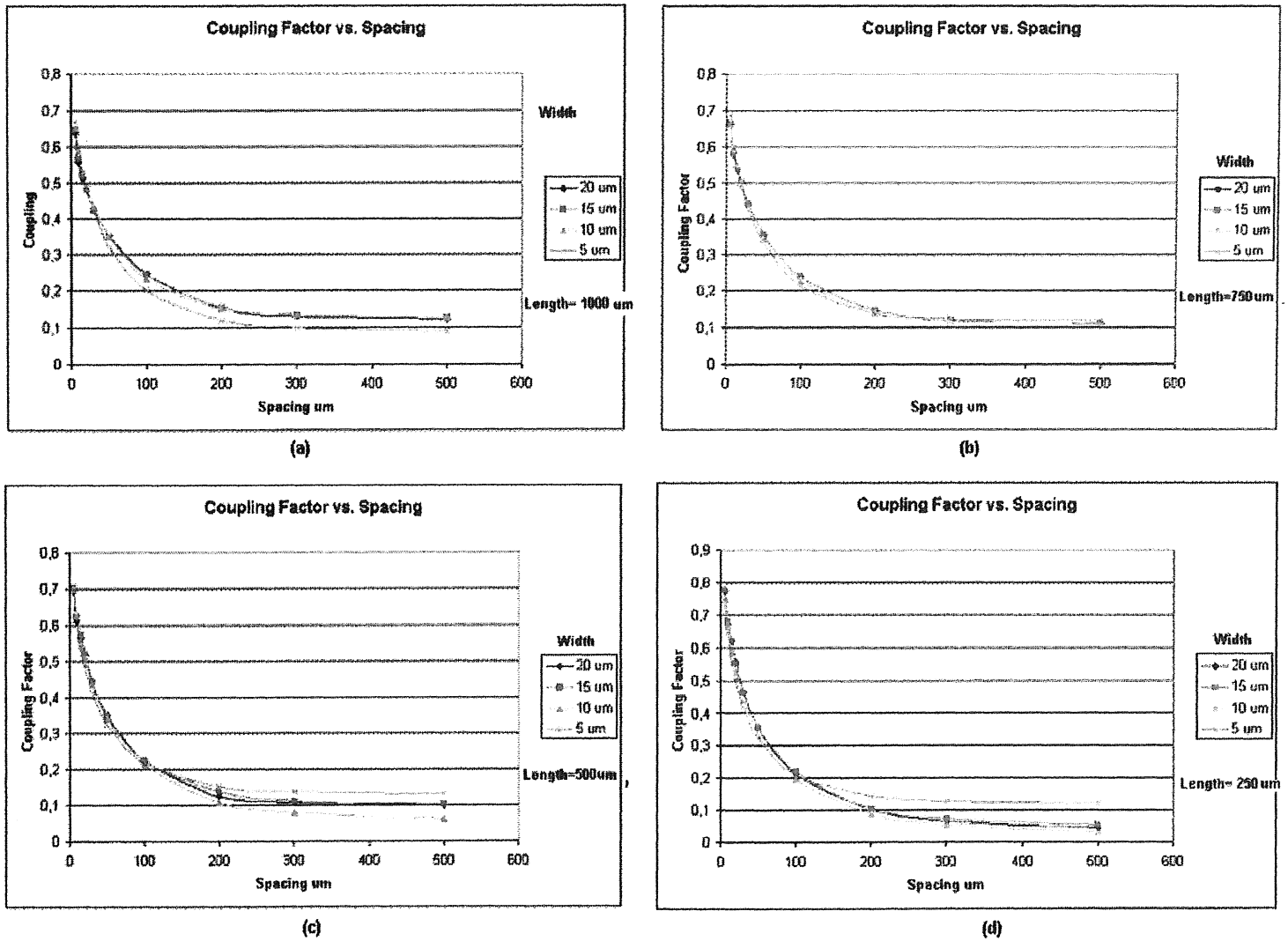

Figure 3.7 The graph of Coupling Factor vs. Spacing um for different lengths (a) 1000 um,(b) 750 um,(c) 500 um and (d) 250 um.

For length 1000 um

Table 3.4
Coefficients of the Coupling Factor for length=1000 um

Width	A	B	C
5 um	0.0926	0.5759	0.0166
10 um	0.1279	0.5231	0.016
15 um	0.1285	0.5192	0.0151
20 um	0.1209	0.5175	0.0142

For length 750 um

Table 3.5
Coefficients of the Coupling Factor for length=750 um

Width	A	B	C
5 um	0.123	0.5624	0.0182
10 um	0.1127	0.5517	0.0157
15 um	0.1138	0.5586	0.015
20 um	0.1122	0.5526	0.0146

For length 500 um

Table 3.6
Coefficients of the Coupling Factor for length=500 um

Width	A	B	C
5 um	0.1333	0.5693	0.0188
10 um	0.0609	0.6378	0.0143
15 um	0.1022	0.6008	0.0159
20 um	0.0091	0.5953	0.0156

For length 250 um

Table 3.7
Coefficients of the Coupling Factor for length=250 um

Width	A	B	C
5 um	0.1209	0.6252	0.0194
10 um	0.0303	0.722	0.0147
15 um	0.0542	0.7207	0.0149
20 um	0.0443	0.7273	0.0146

Now from the above tables we see that A and B are nearly constant for different widths for same length. But they change with change of the length and we have to found the relation how they depend upon length.

By using the curve fitting technique A and B depend upon the length as follows-

$$A = p_1\ell^2 + p_2\ell + p_3 \tag{3.11}$$

$$B = \frac{1}{q_1\ell^2 + q_2\ell + q_3} \tag{3.12}$$

where ℓ is in um and p_1, p_2, p_3, q_1, q_2 and q_3 are the constants which are given as

$$\begin{aligned} p_1 &= 3.2\times10^{-8} & q_1 &= -7.3\times10^{-7} \\ p_2 &= 4.0\times10^{-6} \;\; \& & q_2 &= 0.0016 \\ p_3 &= 0.092 & q_3 &= 1 \end{aligned} \tag{3.13}$$

We find that C depends upon the length and its dependence is given as

$$C = r_1\ell + r_2 \tag{3.14}$$

where ℓ is in um and r_1 and r_2 are the constants given as

$$\begin{aligned} r_1 &= 1.6\times10^{-6} \\ r_2 &= 0.014 \end{aligned} \tag{3.15}$$

3.5 Inter-winding Capacitance

Now we have to calculate the inter-winding capacitance. In this case also from the figure 3.8 we assume that the inter-winding capacitance depends as shown following

$$C_{Coupling} = A_1 + B_1\exp(-C_1 s) \tag{3.16}$$

where $C_{Coupling}$ is the coupling or inter-winding capacitance in pF and s is the spacing between the metal strips in um and where A_1, B_1 and C_1 are functions which depends on the length and width of the strip.

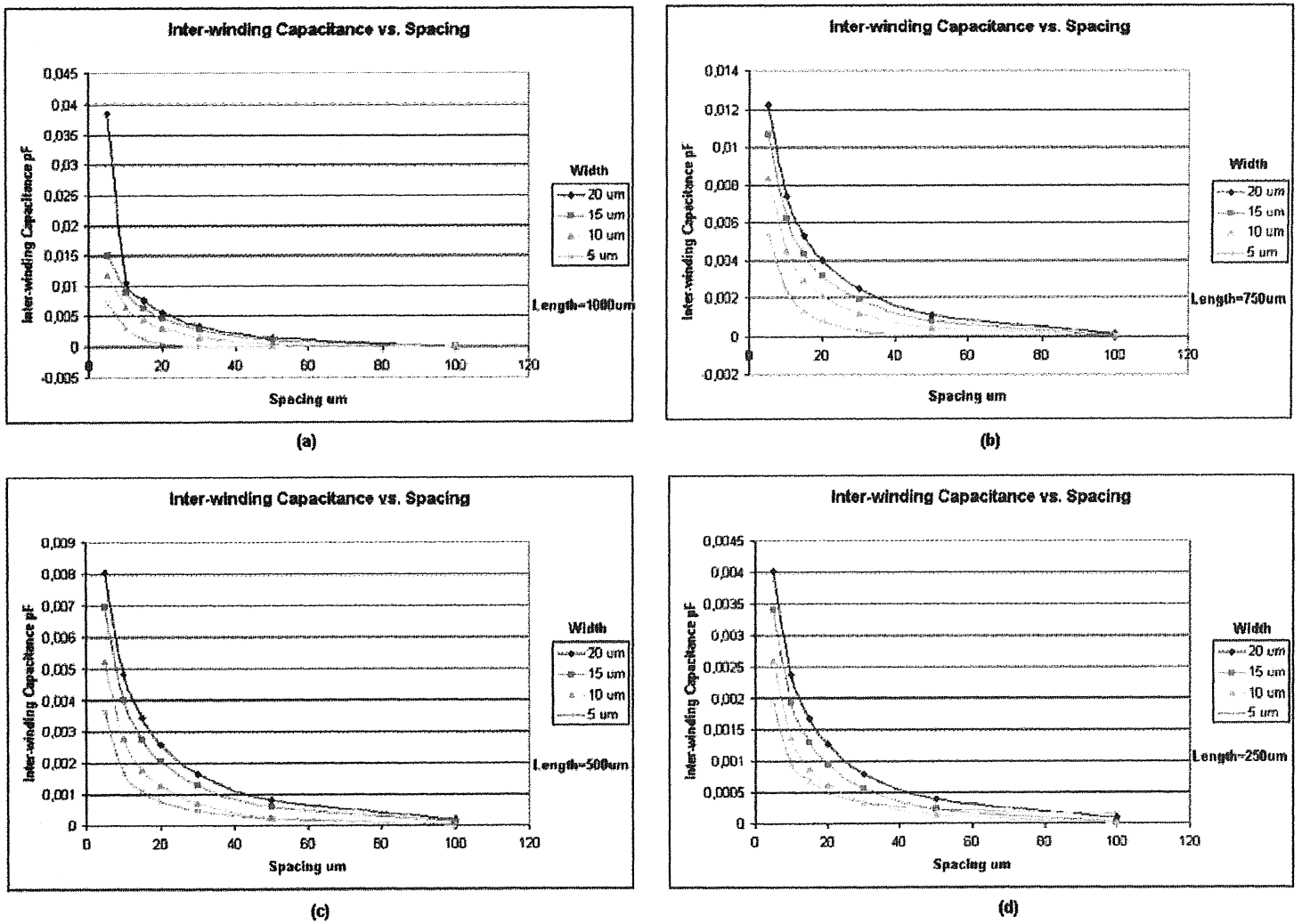

Figure 3.8 The graph of Inter-winding Capacitance vs. Spacing um for different lengths (a) 1000 um,(b) 750 um,(c) 500 um and (d) 250 um

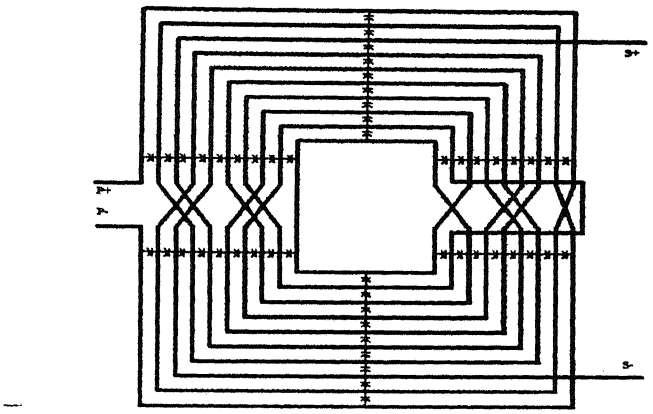

Figure 3.9 Inter-winding Capacitance of a transformer.

The values of A_1,B_1 and C_1 are calculated by using MATLAB

For length 1000 um

Table 3.8
Coefficients of the Inter-winding capacitance for length=1000 um

Width	A_1	B_1	C_1
5 um	4.11e-15	0.0072	0.1369
10 um	7.28e-08	0.0117	0.0666
15 um	1.12e-07	0.0102	0.0414
20 um	1.40e-06	0.0385	0.0961

For length 750 um

Table 3.9
Coefficients of the Inter-winding capacitance for length=750 um

Width	A_1	B_1	C_1
5 um	3.86e-15	0.0054	0.0943
10 um	1.65e-12	0.0084	0.0647
15 um	3.38e-05	0.0106	0.0579
20 um	1.29e-04	0.0121	0.0549

For length 500 um

Table 3.10
Coefficients of the Inter-winding capacitance for length=500 um

Width	A_1	B_1	C_1
5 um	3.92e-05	0.0036	0.0783
10 um	3.58e-07	0.0053	0.0708
15 um	1.26e-04	0.0068	0.0634
20 um	1.98e-04	0.0079	0.0594

For length 250 um

Table 3.11
Coefficients of the Inter-winding capacitance for length=250 um

Width	A_1	B_1	C_1
5 um	1.51e-04	0.0018	-0.0804
10 um	2.40e-08	0.0026	-0.0715
15 um	1.17e-05	0.0034	-0.0643
20 um	9.33e-05	0.0039	-0.0604

We see from the above tables that A_1 is very small so we can neglect it and now we have to find B_1 and C_1.

Here coefficient C_1 can calculated by using the best fitting curve to coupling factor from each spacing shown in the figure 3.8.

Now from the above tables we see that B_1 is the function of length (um) and width (um) and they can be find as following

$$B_1 = (\alpha_1 w^2 + \beta_1 w + \gamma_1)\left(\frac{l}{250}\right)$$
$$C_1 = \frac{1}{\delta w + \xi} \qquad (3.18)$$

where α, β, γ, δ and ξ are the constants which are as follows

$$\alpha_1 = -3.6\times10^{-6}$$
$$\beta = 2.2\times10^{-5} \quad \text{and} \quad \delta = 0.28$$
$$\gamma = 7.7\times10^{-5} \qquad \xi = 11 \qquad (3.19)$$

where $\alpha_1, \beta_1, \gamma_1, \delta$ and ξ are the constants which are as follows:

3.6 Capacitance of the Crossing Area

Since the field distribution in the crossing area is not uniform an accurate value for C_{cr} can only achieved by a 3-dimensional numerical extraction. To save calculation

An first order approximation can be done with the plate capacitor formula

$$C = \frac{\varepsilon A}{d} \tag{3.20}$$

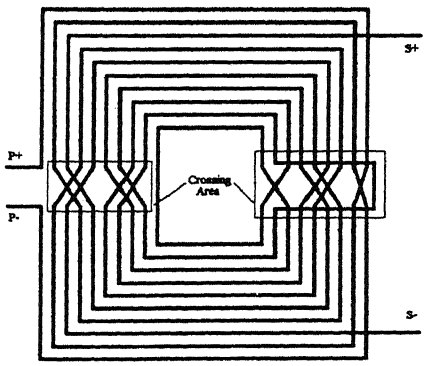

Figure 3.10 Crossing Area Capacitance of a transformer.

Chapter 4

Experimental Results

In this chapter measurement results are compared to simulation results. This is done by an example of an inductor and a transformer in GaAs technology.

The measurements on the transformer and inductor were done with a two port network analyzer in a $Z_0 = 50\ \Omega$ test system. The network analyzer provides the scattering of the test object.

4.1 Measurement Setup

Figure 4.1 shows the on-wafer measurement setup of the transformer / inductor with Network Analyzer and coplanar ground-signal-ground (GSG) probes. During the measurements, the substrate was grounded from the backside of the wafer through testing chuck. The shunt parasitics of the pads in the testing structure were removed in the measurements through using the calibration standards. The S-parameters of the transformer and inductors are measured.

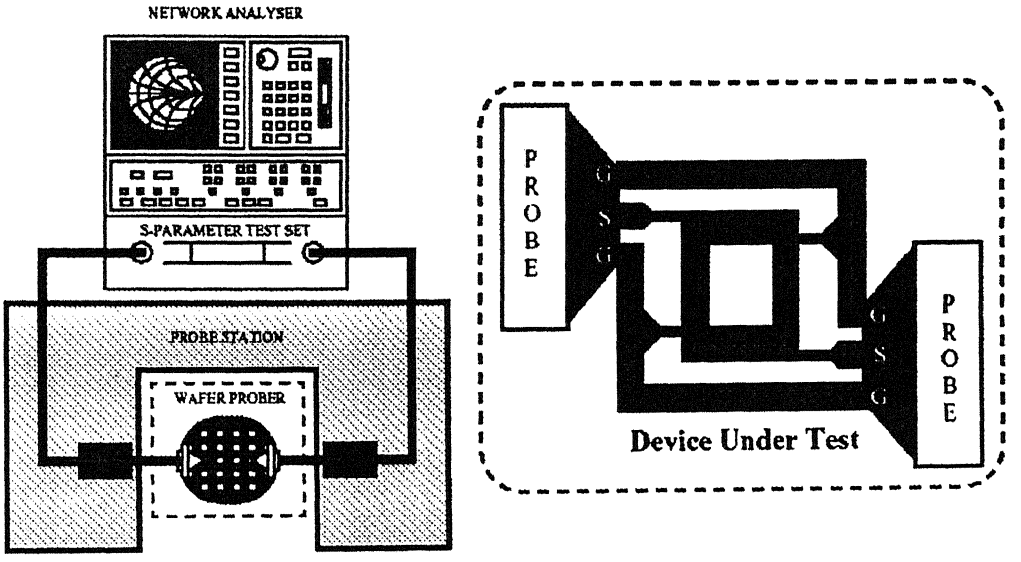

Figure 4.1 Measurement set-up for on-wafer measurement.

4.2 Calibrating Structures Used and De-embedding

Before using monolithic inductors and transformers in integrated circuits it is recommended to characterize their performance by separated measurements. Usually in the RF domain this is done by a network analyzer. The network analyser provides the scattering parameters which describe the electrical behaviour between input and output ports of the test object (DUT) completely. Often these measurements are performed directly on wafer. Although special RF frequency probes are used for this task they cannot be placed directly on the test object. Therefore the test object is embedded in a test structure with defined geometric dimension of the ports. Unfortunately these structures are affected with parasitic inductances and capacitances. They can largely influence the measurement of the actual DUT. In order to obtain the real S-parameters of the DUT the parasitics have to be characterized. Their influences must be subtracted

from the measurement on the test structure .This subtraction procedure is referred to as de-embedding. The following steps show how to get the corrected S-parameters of the DUT. The S-parameters are converted to Y-parameters standardized to Z_0=50 Ω. The conversion in both directions is defined as

$$\begin{aligned} Y &= \frac{1}{Z_0}\left[(E-S)(E+S)^{-1}\right] \\ S &= \left[(E-Z_0Y)(E+Z_0Y)^{-1}\right] \end{aligned} \tag{4.1}$$

where E is the identity matrix with ones on the diagonal and zeros elsewhere.

$$E = \begin{bmatrix} 1 & 0 \\ 0 & 1 \end{bmatrix} \tag{4.2}$$

The conversion from S-parameter to Z-parameter and back is defined as

$$\begin{aligned} Z &= Z_0\left[(E+S)(E-S)^{-1}\right] \\ S &= \left[\left(\frac{Z}{Z_0}-E\right)\left(\frac{Z}{Z_0}+E\right)^{-1}\right] \end{aligned} \tag{4.3}$$

The measured S-parameters of the transformer-structure S corrected with the measured S-parameters of the open structure S_{op} can be calculated as

$$S_{Tr-Op} \leftrightarrow Y_{Tr-Op} = Y - Y_{Op} \tag{4.4}$$

The next step is to correct with measured S-parameters of the short structure S_{Sh}.

$$S_{Tr} \leftrightarrow Z_{Tr} = Z_{Tr-Op} - Z_{Sh} \tag{4.5}$$

S_{Tr} describes the electrical characteristic of the transformer and can be compared to the model. The data of the transformer-structure S in addition to test-structures S_{Sh}, S_{Op} apples after de-embedding the real scattering parameters S_{Tr} of the transformer.

Before these measurements we need to calibrate the network analyser such that it can subtract the parasitics of the probe pads and metal line connections and losses due to cable.

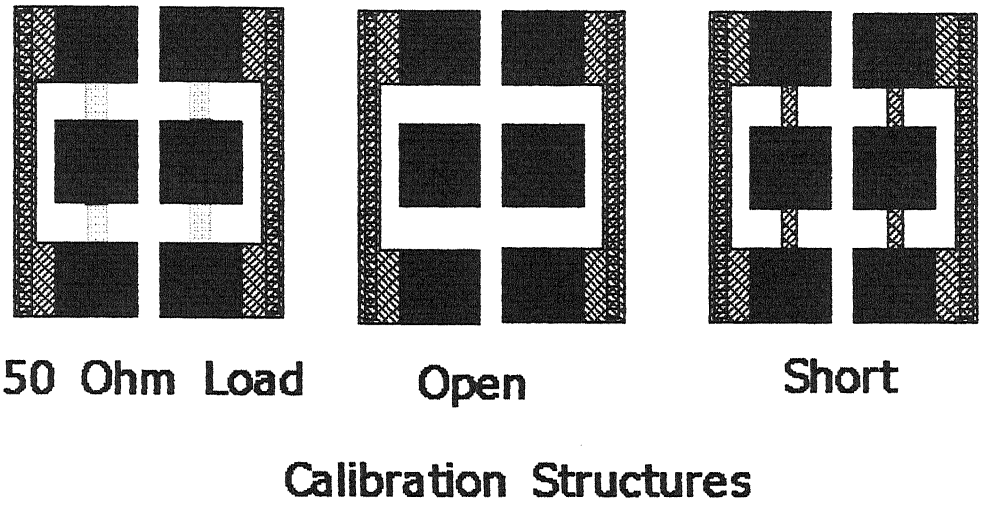

Figure 4.2 Structures used for the calibration of network analyser.

4.3 Inductor I.SY.1

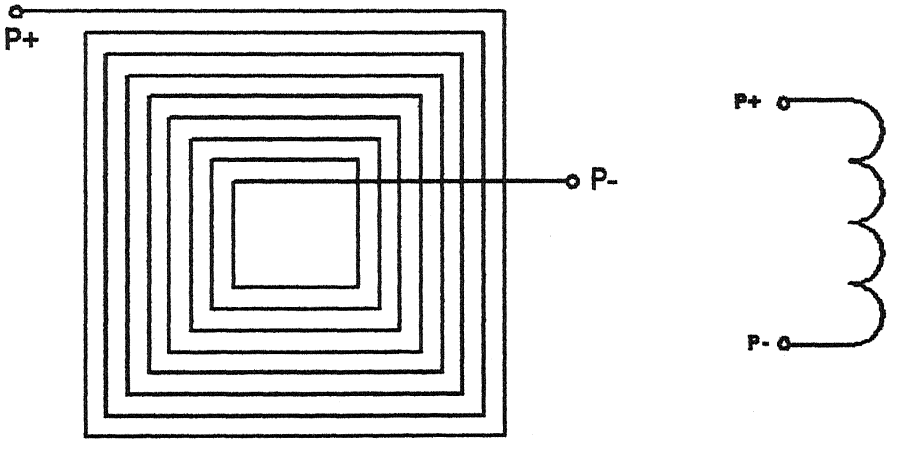

Figure 4.3 Winding scheme of the inductor.

The introduced inductor in this section consists of a symmetrical winding with N=8 and spacing is 5 μm and width also is 5 μm.

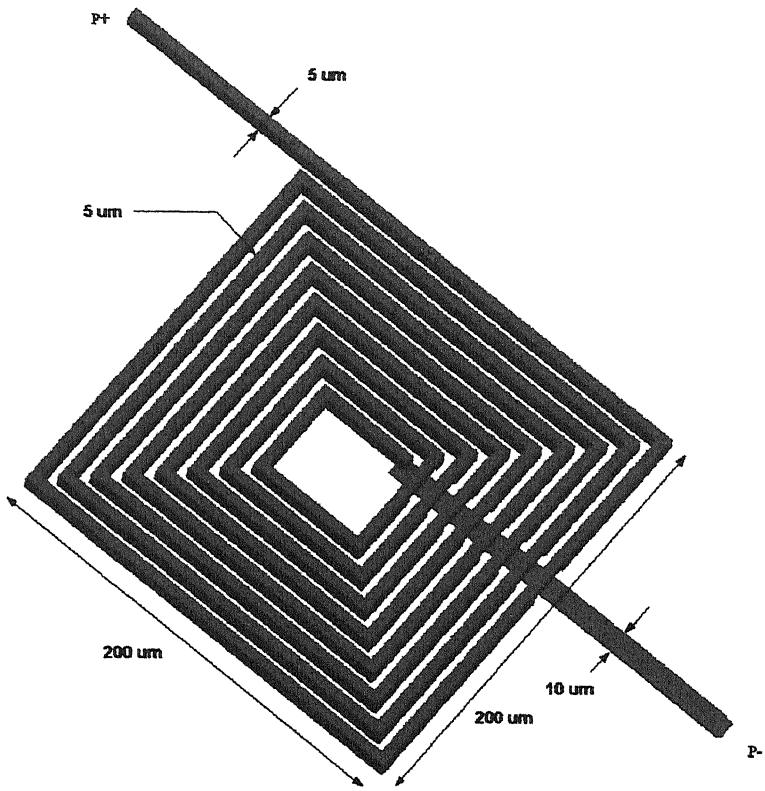

Figure 4.4 Design of Inductor I.SY.1.

Figure 4.5 shows the scattering parameter S11 of the inductor. S11 represents the input reflection coefficient. S11 is simulated and measured in a frequency range between f = 1 GHz and f = 10 GHz.

Figure 4.6 and 4.7 show the real and imaginary part of the reciprocal of the admittance parameter Y11. The curves gives the information about the input impedance of the inductor when the second port is shorten to ground. This is a very important

exciting mode of the inductor which is often used in applications. The maximum value of the real part indicates

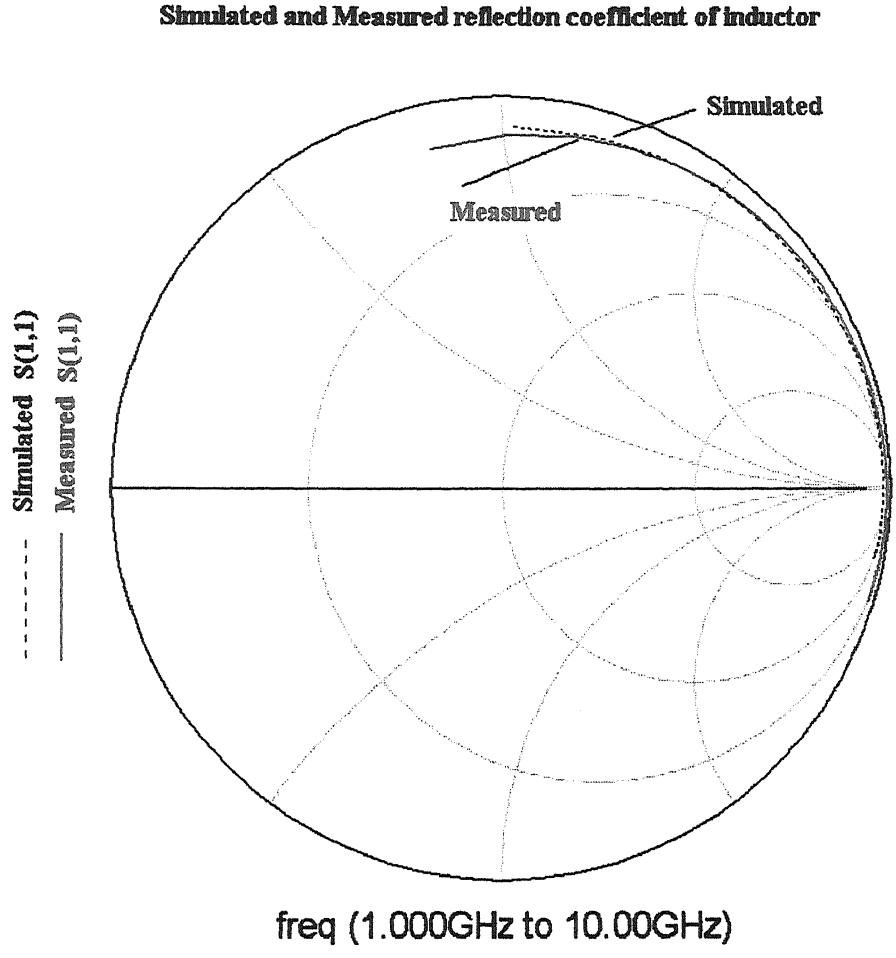

Figure 4.5 Simulated and measured reflection coefficient of inductor.

the parallel resonant frequency of the inductor. The predicted resonant frequency from the model is at 7.330 GHz is close to measured at 7.340 GHz.

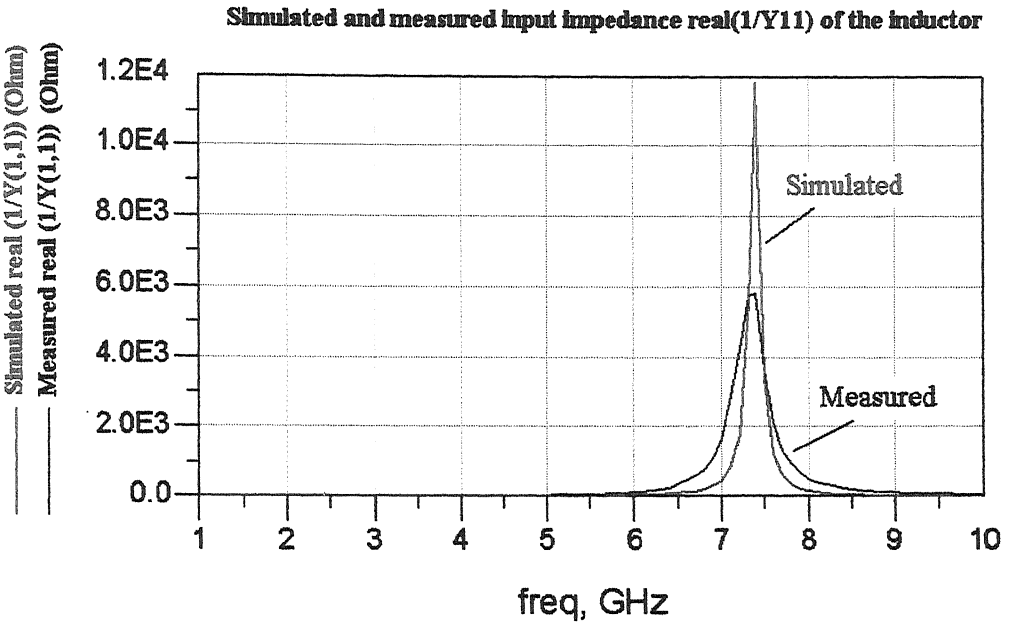

Figure 4.6 Simulated and measured input impedance real(1/Y11) of the inductor.

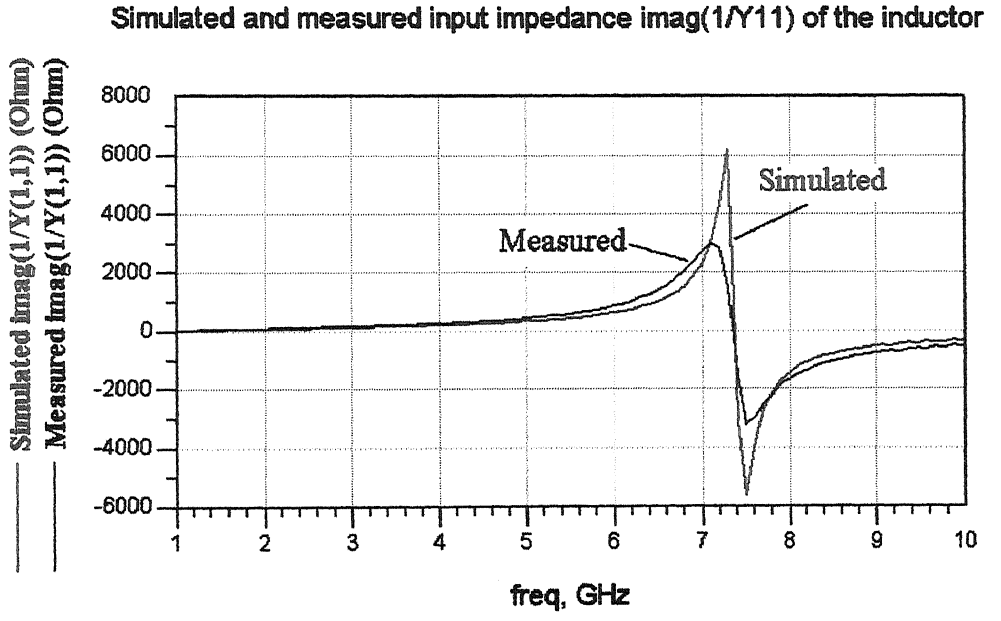

Figure 4.7 Simulated and measured input impedance imag(1/Y11) of the inductor.

Figure 4.8 shows the effective inductance between the two ports of the inductor over the frequency. The inductance can be extracted from the input resistance at shorten output by

$$L = \frac{imag\left(Y_{11}^{-1}\right)}{\omega} \tag{4.6}$$

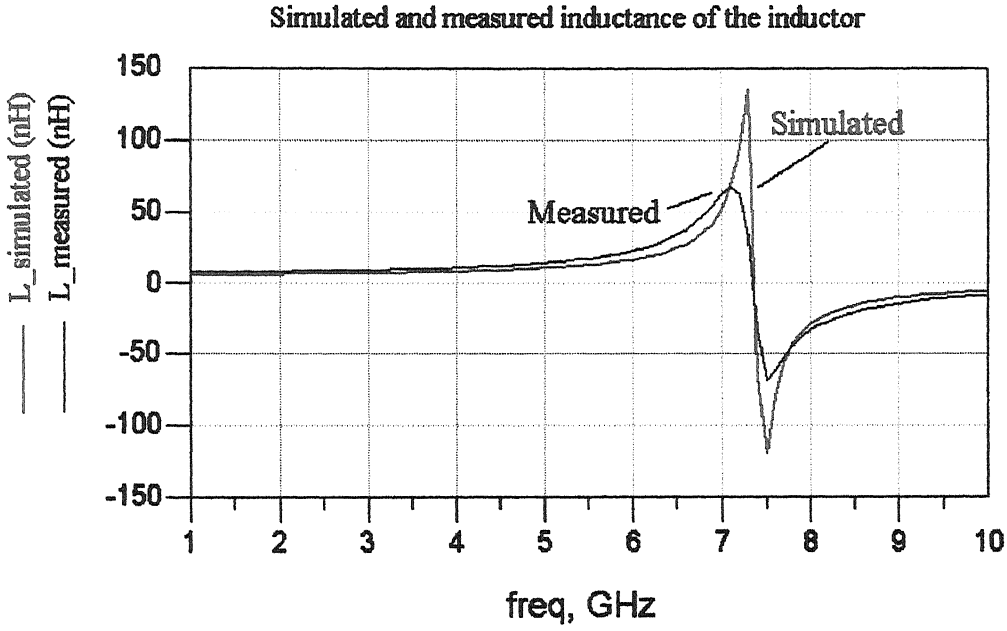

Figure 4.8 Simulated and measured inductance of the inductor.

A good match is observed between the measurement and the simulated model. Note, the inductor changes its sign at resonant frequency to negative. That implies that the inductor loses its inductive character. Hence, after the resonant frequency the device acts as a capacitor rather than an inductor.

4.4 Transformer T.SY.V1

The transformer is realized with two planar symmetrical windings. The primary winding consists of 5 turns and the secondary also of 5 turns. Additionally, the secondary winding has a centre-tap which allows a usage in the balanced applications. An application of this transformer has been given in the introduction chapter. It is used in the mixer. Figure 4.9 shows the winding scheme of the transformer and figure 4.10 shows the structure of transformer.

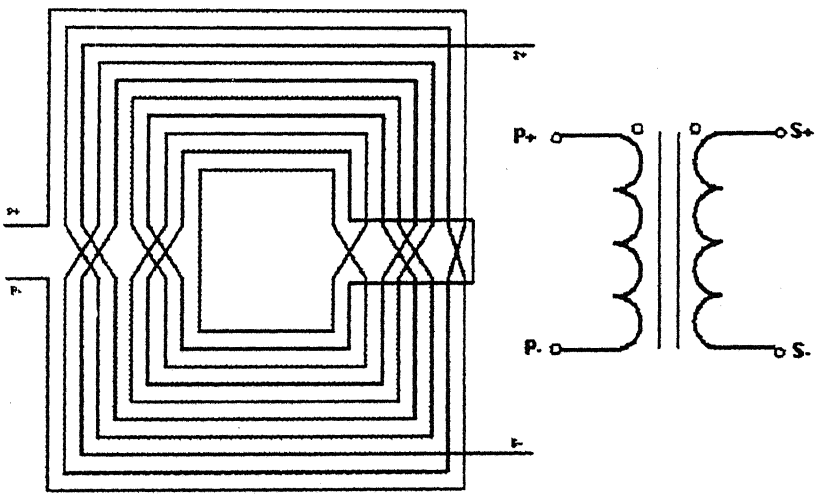

Figure 4.9 Winding scheme of the transformer T.SY.V1.

Figure 4.11 and 4.12 illustrate the reflection and transmission factor of the two port transformer. Where port1 is related to primary side and port2 to the secondary side of the transformer as figure 4.8. The centre-tap on the secondary is left open and therefore not taken into consideration for the measurements.

The simulated scattering parameters didn't show good agreement to the measured data in the frequency range but its shape of the simulated of scattering parameters is much similar to that of the measured scattering parameters. This deviation between the model prediction and measurement is because of more complex structure of transformer and more number of elements used in the model.

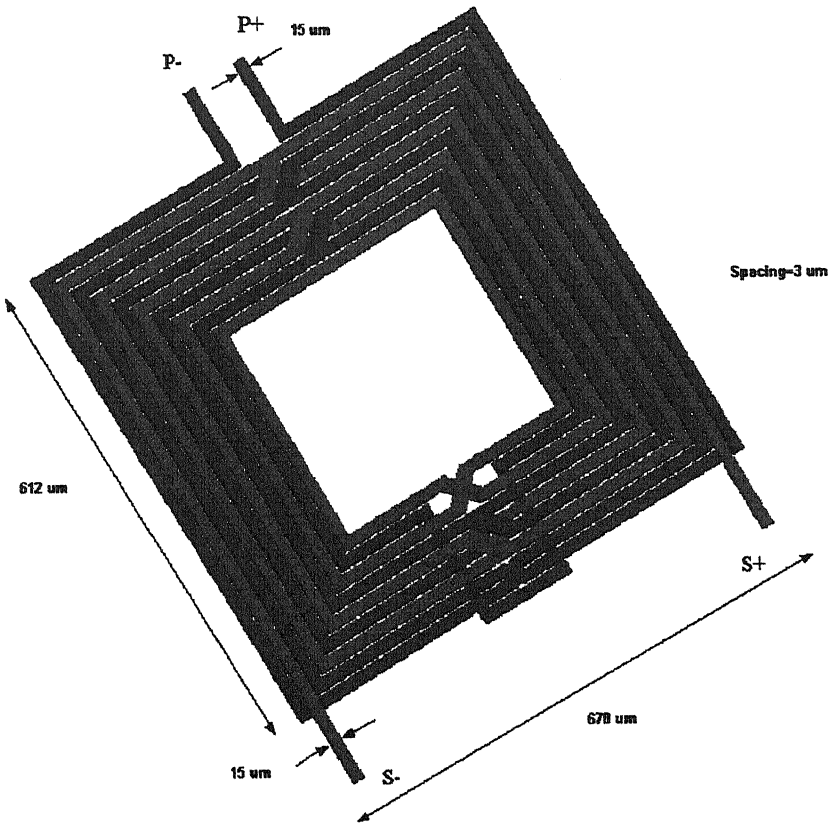

Figure 4.10 Structure of transformer

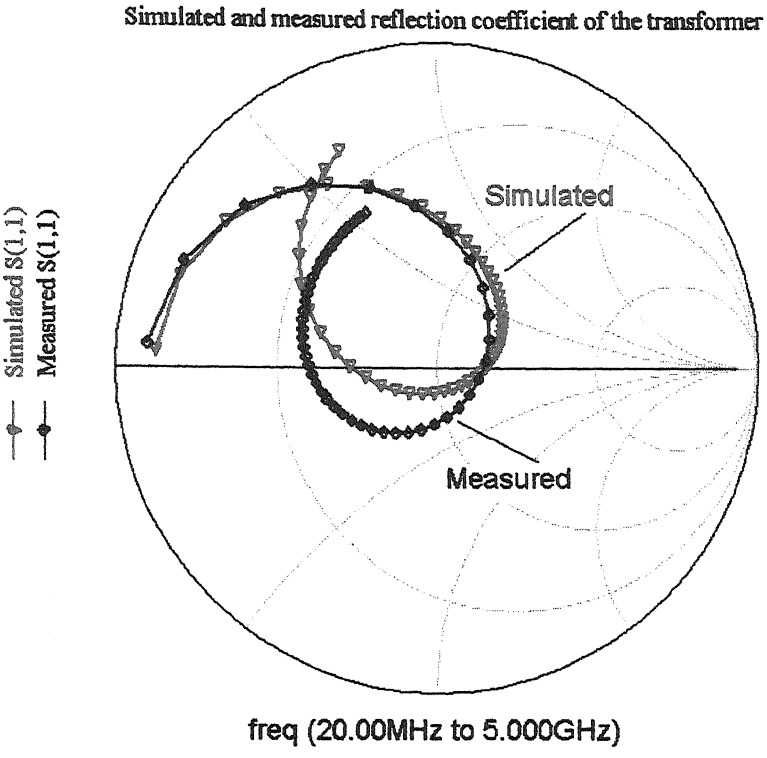

Figure 4.11 Simulated and measured reflection coefficient of the transformer.

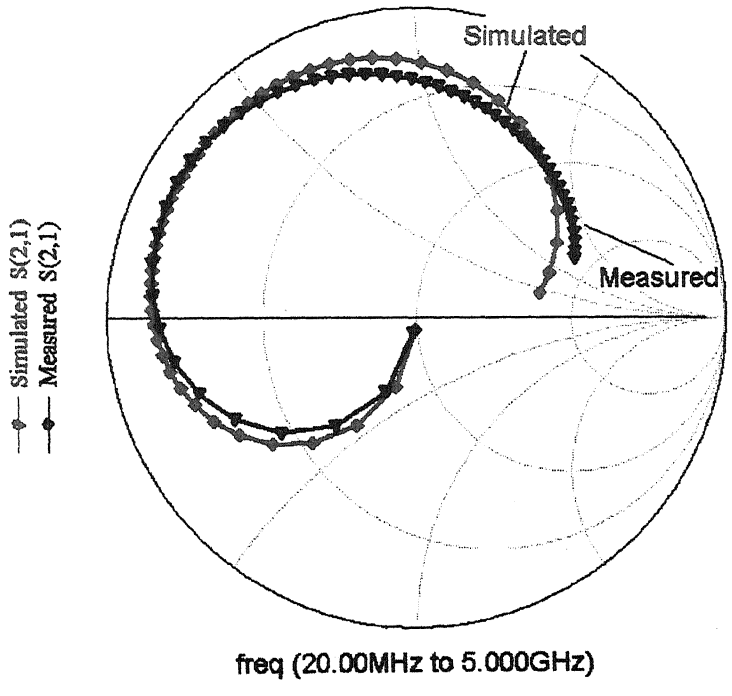

Figure 4.12 Simulated and measured transmission coefficient of the transformer.

Chapter 5

Applications of Transformers in RF Integrated Circuits

5.1 Application

Some of the typical applications of on-chip transformers have been mentioned in the introduction of Chapter 1. Take, for example, the design of a RF mixer which employs an on-chip transformers and diodes.

5.2 Mixers

5.2.1 Introduction

All electronic circuits are nonlinear, this is a fundamental point of electronic engineering. In some circuits, nonlinearities are weak and can be neglected, in others effects must be minimized in order to avoid bad operating, but some circuits like mixers and frequencies multipliers need nonlinearities to operate. In our study we will interest us in mixers performance. Mixers performance measures such as conversion gain, gain compression, intercept and inter-modulation and isolation will be explained.

5.2.2 Mixer Basics

A mixer is a circuit which performs a frequency translation either from a high frequency input signal to a low frequency output signal or vice versa. Applying a high frequency signal and a high frequency local oscillator signal performs a frequency translation to low frequencies. The output signal of interest is at the frequency f_{IF}

(Intermediary Frequency), which is the difference of the input signal frequency (f_{RF}) and the local oscillator frequency (f_{LO}). This kind of frequency translation is used in receiver circuits and is referred as downconversion as shown in figure 5.1.

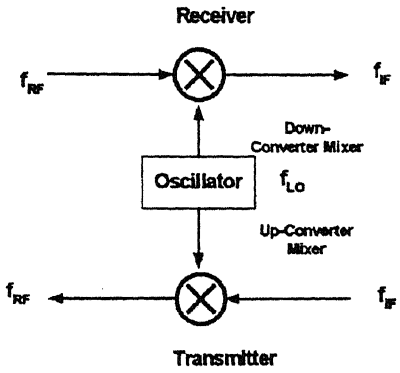

Figure 5.1 Mixer Structure.

The opposite of it, frequency translation to high frequencies is referred as up conversion.

The mixer is a nonlinear component, which will generate mixing products following the principles of nonlinearity we will explain in detail. The sinusoidal LO signal leads to periodic variation of RF control voltage of nonlinear device (for example a transistor) and will generate nonlinear variations of element values of device.

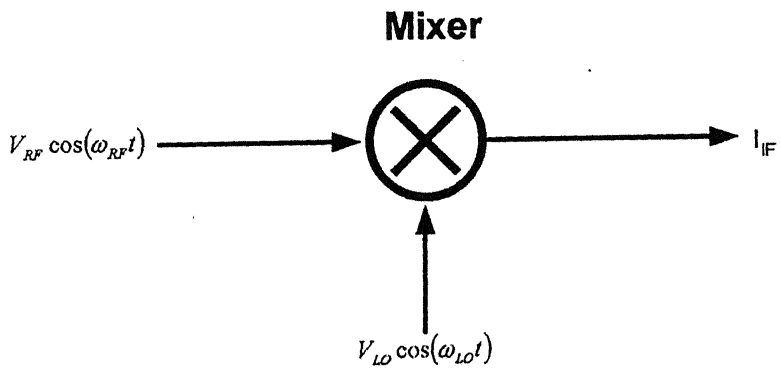

Figure 5.2 Mixer Symbol.

Figure 5.2 shows the symbolic schematic of a mixer.

The mixer acts as a signal combiner and the output voltage is a function of V_{LO} and V_{RF}, for the moment we assume that the output voltage is simply:

$$V_{IF}(t) = V_{LO}\cos(\omega_{LO}t) + V_{RF}\cos(\omega_{RF}t) \qquad (5.1)$$

The output current is $I_{IF} = f(V_{IF}) = f(V_{LO}, V_{RF})$, then, using a nonlinear component to make the mixer, I_{IF} will be a nonlinear function of V_{IF} and then of V_{LO} and V_{RF}.

5.2.3 Description of non-linearity

Linear circuits are characterized by the following property: if excitations x_1 and x_2 are applied separately to a circuit having y_1 and y_2 for responses respectively, the response to the excitation ax_1+bx_2 is ay_1+by_2, where a and b are arbitrary constants. An important point is that the response of such circuits will only include the frequencies present in the excitation waveforms and not generate new frequencies. In nonlinear circuits the output does not vary linearly with the input and remarkably large number of new frequencies are generated. In addition nonlinear circuits are often characterized as either weakly nonlinear or strongly nonlinear. A weakly nonlinear circuit can be described with adequate accuracy by a power series expansion of its nonlinear current/voltage characteristic (I/V). This definition implies that the characteristic is continuous, has continuous derivatives and for most purpose does not require more than few terms in the power series. The excitation level, which affects the number of power

series terms required, must also not be too high. Virtually, all passive components and transistors satisfy this definition if the excitation voltages are well within the components' normal operating ranges.[13]

Strongly nonlinear components are all those that do not fit the definition of weakly nonlinearity, for example strongly driven transistors or Schottky diodes because of their exponential characteristics. Now we will explain how new frequencies are generated in a nonlinear circuit. Figure 5.3 shows a nonlinear resistor, which can symbolise the operation of a mixer. V_{IF} is the command voltage and I_{IF} the response.

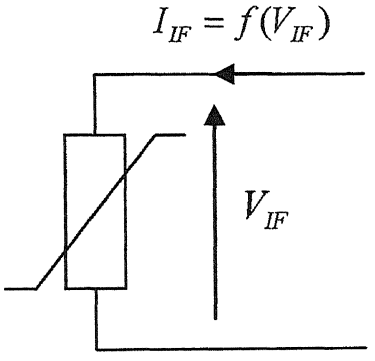

Figure 5.3 A nonlinear resistor.

Assume that the relationship between the command signal V_{IF} and the response signal I_{IF} is-

$$I_{IF} = K_1 V_{IF} + K_2 V_{IF}^2 + K_3 V_{IF}^3 + \ldots + K_n V_{IF}^n \qquad (5.2)$$

When the input-output relationship is given by an analytic relationship $I_{IF} = f(V_{IF})$ then the coefficients $K_1, K_2, K_3, \ldots$ can be identified with the coefficients of

$$K_1 = \frac{df}{dV_{IF}} \qquad K_2 = \frac{1}{2}\frac{d^2 f}{dV_{IF}^2}$$

$$K_3 = \frac{1}{6}\frac{d^3 f}{dV_{IF}^3} \quad \ldots\ldots \qquad K_n = \frac{1}{n!}\frac{d^n f}{dV_{IF}^n}. \tag{5.3}$$

Coefficient K_1 describes the behaviour of the linearized circuit, K_2 and K_3 are respectively called second and third order nonlinearity coefficients of the circuit. They determine the second and the third order nonlinear circuit behaviour. As we said before, we assume that

$$V_{IF}(t) = V_{LO}\cos(\omega_{LO}t) + V_{RF}\cos(\omega_{RF}t) \tag{5.4}$$

Substituting the value of V_{IF} into i_{K1} gives, for the first term,

$$i_{K_1}(t) = K_1 V_{IF}(t) = K_1 V_{LO}\cos(\omega_{LO}t) + K_1 V_{RF}\cos(\omega_{RF}t) \tag{5.5}$$

Doing the same operation for the second term (the quadratic) and applying trigonometric formulas for squares and products of cosines we obtain

$$\begin{aligned} i_{K_2}(t) &= K_2 V_{IF}^2(t) \\ &= \frac{1}{2}K_2\left[\begin{array}{l} V_{LO}^2 + V_{RF}^2 + V_{LO}^2\cos(2\omega_{LO}t) + V_{RF}^2\cos(2\omega_{RF}t) \\ + 2V_{LO}V_{RF}\left[\cos((\omega_{LO}+\omega_{RF})t) + \cos((\omega_{LO}-\omega_{RF})t)\right] \end{array}\right] \end{aligned} \tag{5.6}$$

And the third term (the cubic) gives:

$$i_{K_3}(t) = K_3 V_{IF}^3(t)$$

$$= \frac{1}{4} K_3 \begin{bmatrix} V_{LO}^3 \cos(3\omega_{LO}t) + V_{RF}^3 \cos(3\omega_{RF}t) \\ + 3V_{LO}^2 V_{RF}[\cos((2\omega_{LO} + \omega_{RF})t) + \cos((2\omega_{LO} - \omega_{RF})t)] \\ + 3V_{LO} V_{RF}^2[\cos((2\omega_{RF} + \omega_{LO})t) + \cos((2\omega_{RF} - \omega_{LO})t)] \\ + 3(V_{LO}^3 + 2V_{LO}V_{RF}^2)\cos(\omega_{LO}t) \\ + 3(V_{RF}^3 + 2V_{LO}^2 V_{RF})\cos(\omega_{RF}t) \end{bmatrix} \quad (5.7)$$

The total current in the nonlinear element is the sum of the different current components $i_{K_1}, i_{K_2}, i_{K_3} \ldots i_{K_n}$

All the generated frequencies occur for linear combinations of the two excitation frequencies, indeed $\omega_{n,m} = m\omega_{LO} + n\omega_{RF}$ where m, n = ...-3, -2, -1,0,1,2,3.....

$\omega_{n,m}$ is called mixing frequency (or intermodulation frequency), the current at that frequency is called mixing product and $k = |m| + |n|$ is the order of intermodulation.

$\omega_{0,m}$ and $\omega_{n,0}$(with m>1 and n>1) are the harmonics of the excitation frequencies. Fundamental frequencies are $\omega_{0,1}$ and $\omega_{1,0}$.

In the case of a mixer, mixing frequencies of interest are $\omega_{1,-1}$ (which corresponds to Intermediate Frequency) for downconversion and $\omega_{1,1}$ for upconversion; these frequencies are the second order-mixing products.

We underline that the response signal at ω_{LO} and ω_{RF} depends on K_1 and K_3, thus the signs of these coefficients determine if the nonlinearity acts as a compression (K_1 and K_3 have opposite sign) or an expansion (K_1 and K_3 have the same sign).

Figure 5.4 shows the spectrum of I_{IF} until third order of intermodulation, we assume that LO and RF signal have the same excitation amplitude V.

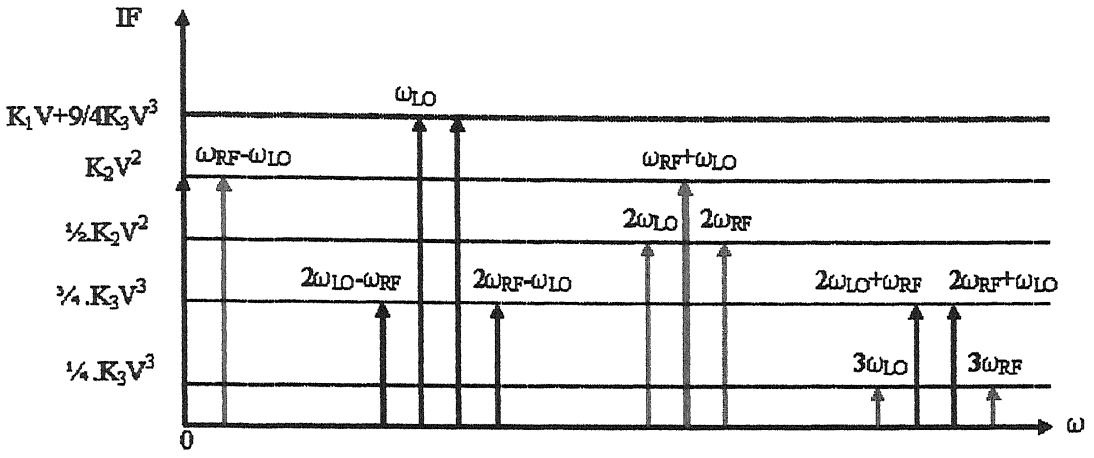

Figure 5.4 The different frequency components at the IF port of a mixer.

5.2.4 Nonlinear effects in electrical circuits

The following definitions of parameters will be useful to study and quantify nonlinearities in a circuit.

As our aim is to deal with mixers and particularly with down mixers, we consider the following definitions for a circuit excited by two sinusoids (LO and RF signals) but it is also possible to apply them to a one frequency excited circuit. In this case there are no mixing products but only harmonics of the fundamental frequency. On the other hand it is also possible to have more than one RF signal.

5.2.4.1 Conversion Gain

As we said before, the output signal of interest in a mixer is the second order mixing product which is at the frequency $f_{IF} = f_{RF} - f_{LO}$ (we assume that $f_{RF} > f_{LO}$) for a down converter, therefore the conversion gain is defined as the ratio $\frac{P_{IF}}{P_{RF}}$.

P_{IF} is the power of the IF signal (at IF frequency) and P_{RF} is the power of the RF signal (available power).

If the powers are given in dB or dBm, the conversion gain is of course the difference between P_{IF} and P_{RF}. When this gain is negative it is also called conversion loss.

5.2.4.2 Compression Point

Referring to Figure 5.5 it is seen that from a certain input level, the fundamental response does not increase anymore proportionally with the input level.

The gain (and the conversion gain) is compressed and a quantitative measurement for this gain compression is the 1 dB compression point, which is no ted P1dB on Figure 5.5. This figure indicates the input level for which the fundamental is 1 dB lower than the extrapolation of the response at lower amplitudes, which is caused by linear behaviour only.

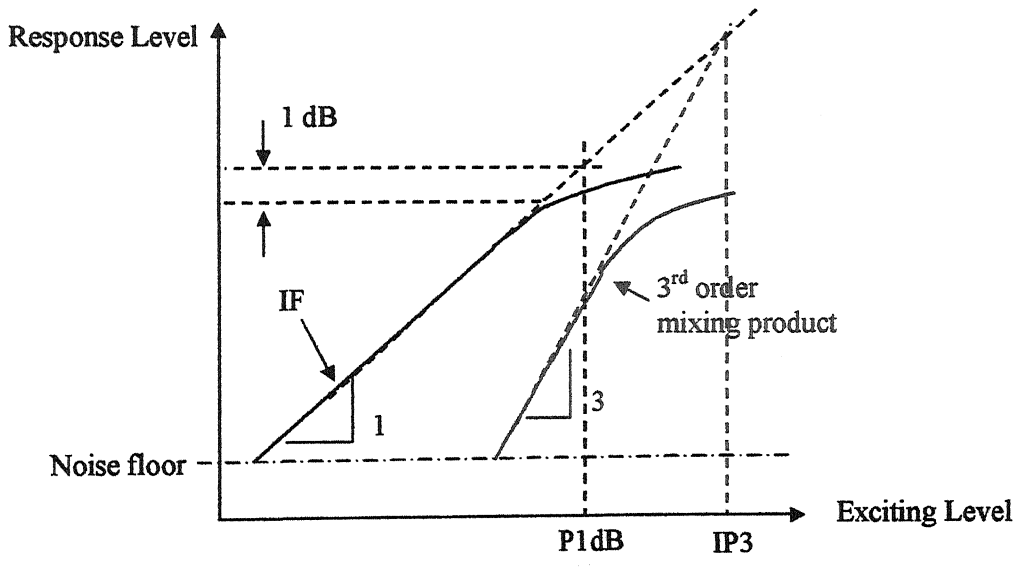

Figure 5.5 Illustration of 1 dB compression and third order intercept point .

5.4.2.3 Intercept Points

Intercept points are defined when two RF (RF1 and RF2) signals are applied. The frequencies of these signals f_{RF1} and f_{RF2} are the fundamental frequencies. Figure 5.6 shows the spectrum of these signals .In this case the terms at IF1 and IF2 frequencies are the first order mixing products. The third order-mixing products are at $2f_{RF1}-f_{RF2}-f_{LO}$ (IM31) and $2f_{RF2}-f_{RF1}-f_{LO}$ (IM32). The response at these frequencies increases with a slope of 3 dB/dec. whereas the responses at IF1 and IF2 frequencies increase linearly with the exciting amplitude. Since the third order mixing product increases faster with the exciting level as the first order mixing product response due to a linear behaviour, the extrapolation of both curves must intersect (Figure 5.5.).The exciting level corresponding to this intersection is called input third order intercept point IIP3, the response level is called output third order intercept point OIP3. In our report we will only speak about input third order intercept point and we will call it simply IP3. The higher this intercept point is, the better of course the second order mixing product is suppressed and the most linear the circuit is.

Similarly we can define an n^{th} order intercept point IPn.

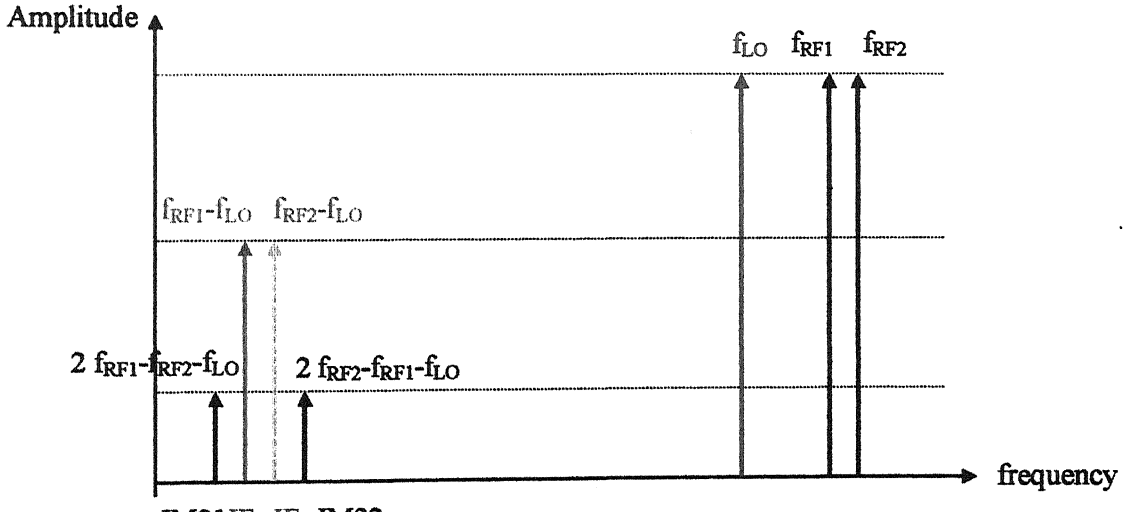

Figure 5.6 Output spectrum of a mixer.

A simple formula exists for calculating input intercept point, given the level of intermodulation suppression, the order of the intermodulation, and the input RF power levels giving rise to this level of suppression.

$$IIP = \frac{\text{Intermodulation suppression (dBc)}}{\text{(order -1)}} + \text{[input RF power (dBm)]} \quad (5.8)$$

For example, if each input tone has -10 dBm of power, and the third-order, two-tone intermodulation suppression is 46 dBc, then the IIP is

$$IIP = \frac{46}{3-1} + (-10\ \text{dBm}) = +13\ \text{dBm}$$

Also, output and input intercept are related by the mixer conversion loss, or gain (for active mixers).

$$OIP(dBm) = IIP(dBm) \begin{cases} - \ mixer \ conversion \ loss \ (dB), \ or \\ + \ mixer \ conversion \ gain \ (dB) \end{cases} \quad (5.9)$$

5.3 Design of Mixer

We have used the diode ring double-balanced mixer.

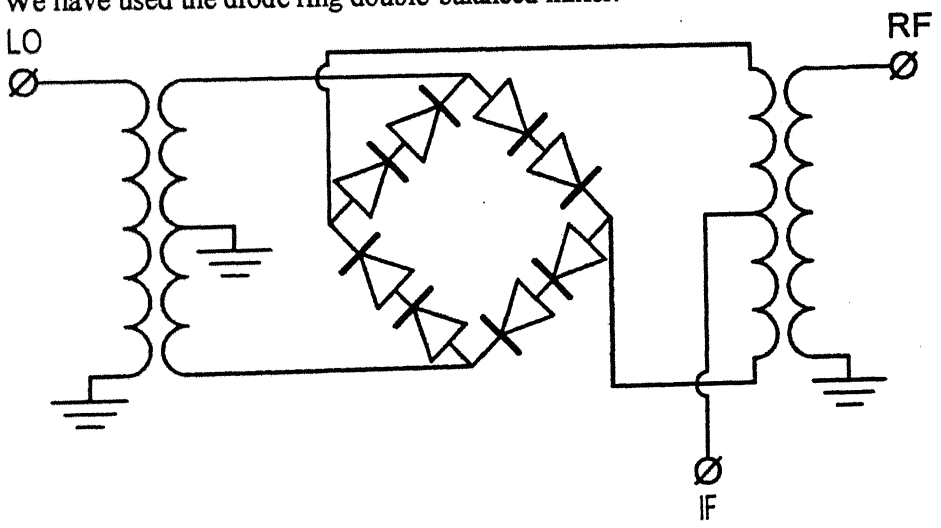

Figure 5.7 Double Balanced Diode Ring Mixer.

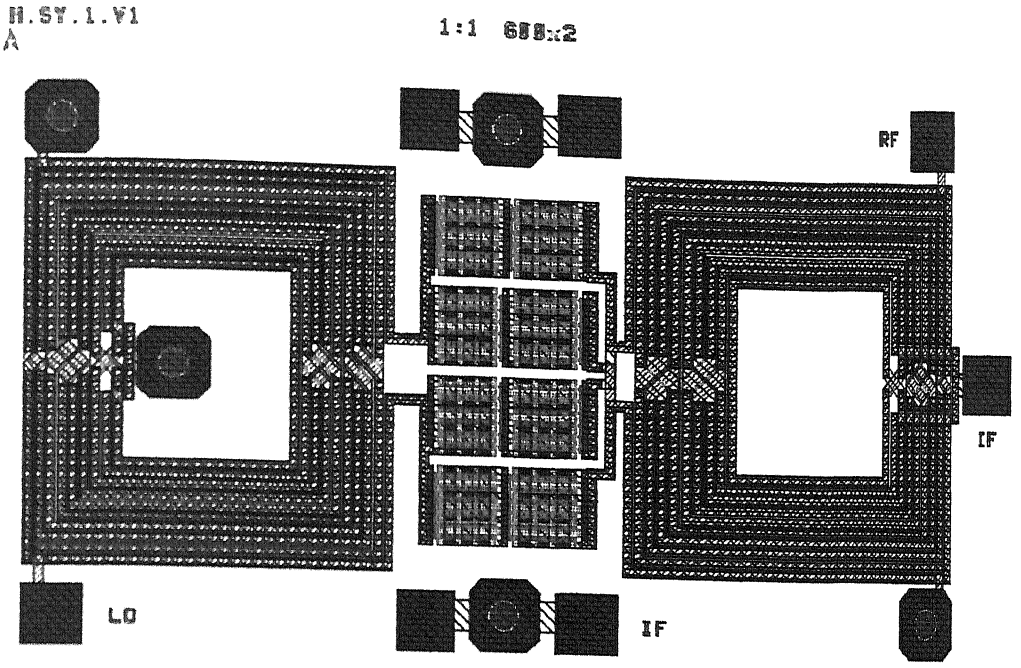

Figure 5.8 Layout of Double Balanced Diode Ring Mixer.

5.4 Measurement Results

A 0 dBm input signal is applied to the RF port. We have measured the 1 dB compression point for P_{LO} = 19 dBm. IF=100 MHz.

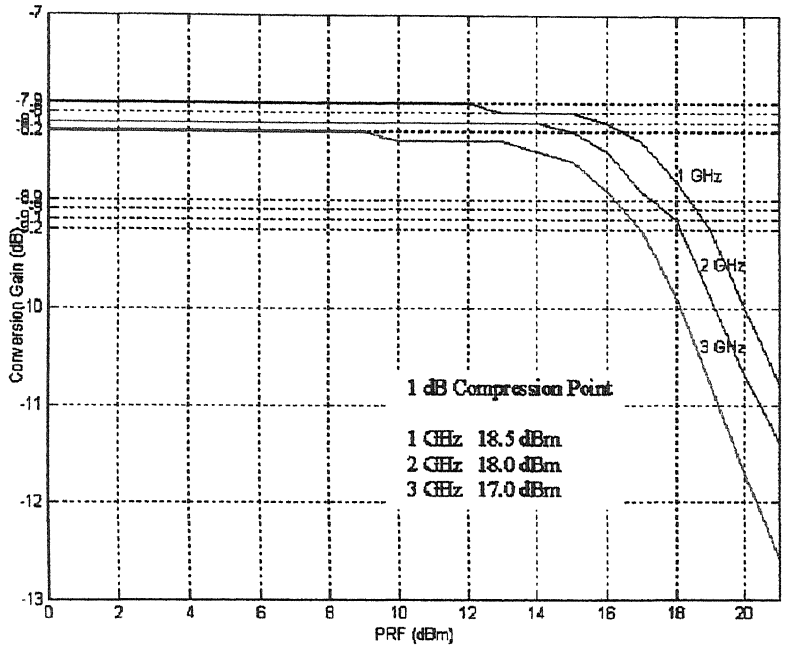

Figure 5.9 Conversion Gain(dB) vs. PRF (dBm).

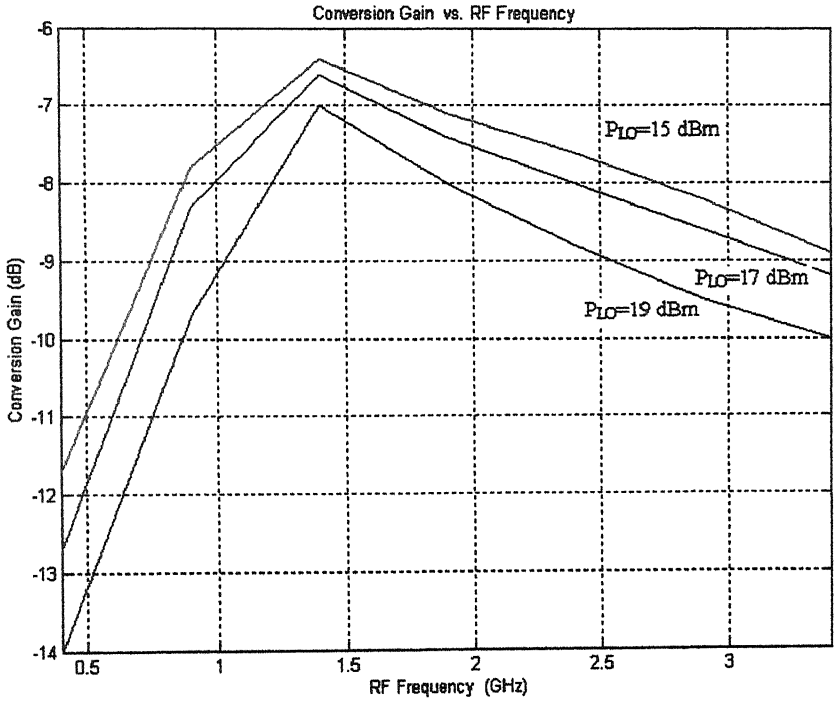

Figure 5.10 Conversion Gain (dB) vs. RF Frequency (GHz).

IIP3 Calculations for different Input Power Levels
For 1 GHz

Table 5.1
IIP3 Calculations for 1 GHz

Pin	Intermodulation Suppression Δ (dB)	IIP3=Pin+Δ/2
0 dBm	60.00	30.00 dBm
1 dBm	58.00	30.00 dBm
2 dBm	56.70	30.35 dBm

For 2 GHz

Table 5.2
IIP3 Calculations for 2 GHz

Pin	Intermodulation Suppression Δ (dB)	IIP3=Pin+Δ/2
0 dBm	59.00	29.50 dBm
1 dBm	57.00	29.50 dBm
2 dBm	55.00	29.50 dBm

For 3 GHz

Table 5.3
IIP3 Calculations for 3 GHz

Pin	Intermodulation Suppression Δ (dB)	IIP3=Pin+Δ/2
0 dBm	60.00	30.50 dBm
1 dBm	58.00	30.50 dBm
2 dBm	56.70	30.50 dBm

Chapter 6

High Performance Inductors

In this chapter, we will describe the design and analysis of several square inductors on GaAs substrates. It has been shown experimentally that the quality factor of spiral inductors can be increased by reducing magnetically induced currents and by narrowing the line width of the inner turns similar to the one reported for silicon micro-machined inductor. Using this technique we observed about 5-10 % improvement in the quality factor of spiral inductors having constant line width.

6.1 Quality Factor

Several different definitions of Q-factors for inductors have been used in the literature [14-19]. The most general definition of Q is based on the ratio of energy stored, W_S, to power dissipated, P_D, in the inductor per cycle; that is

$$Q = \frac{\omega W_S}{P_D} \tag{6.1}$$

At low frequencies an inductor's primary reactance is inductive and

$$Q = \frac{\omega \frac{1}{2} L i_0^2}{\frac{1}{2} R i_0^2} = \frac{\omega L}{R} \quad Q = \frac{\omega W_S}{P_D} \tag{6.2}$$

where i_0 is the rms value of the current. When the inductor is used as a resonant component close to its resonance frequency (SRF) f_{res}, a more appropriate definition of the Q-factor is in terms of its 3-dB bandwidth (BW)is given by

$$Q = \frac{f_{res}}{BW} \; Q = \frac{\omega W_S}{P_D} \tag{6.3}$$

A third definition of Q-factor, which has been used for distributed resonators, is evaluated from the rate of change of input reactance with frequency [19]:

$$Q = \frac{f_{res}}{2R}\left[\frac{dX_{in}}{df}\right] \tag{6.4}$$

where X_{in} is the input reactance of the inductor and $\frac{dX_{in}}{df}$ is determined at f_{res}.

In microwave circuits where the inductors are used far below the self-resonance frequency, the degree at which the inductor deviates from an ideal component is described by the effective quality factor Q_{eff} is expressed as :

$$Q_{eff} = \frac{\mathrm{Im}[Z_{in}]}{\mathrm{Re}[Z_{in}]} = \frac{X}{R} = \frac{\omega L_e}{R} \tag{6.5}$$

where $\mathrm{Re}[Z_{in}]$ and $\mathrm{Im}[Z_{in}]$ are the real and imaginary parts of the input impedance of the inductor, respectively. This definition leads to the unusual condition that Q_{eff} becomes zero at resonance. Since in RF and microwave circuits, for series applications of inductors, the operating frequencies are well below the self resonance frequency, the preceding definition is traditionally accepted.

6.2 Self Resonance Frequency

The self resonance frequency (f_{res}) of an inductor is determined when $Im[Z_{in}]=0$; that is, the inductive reactance and the parasitic capacitive reactance become equal and opposite in sign. At this point, $Re[Z_{in}]$ is maximum due to parallel resonance and the angle of Z_{in} changes the sign. The inductor's first resonant frequency is of the parallel resonance type. Beyond the resonant frequency, the inductor becomes capacitive.

6.3 Q Enhancement Techniques

One of the important characteristics of an inductor on a GaAs substrate is its quality factor Q. Higher values of Q are needed to improve the microwave circuit's performance. Techniques used to enhance the Q-factor of inductors on a GaAs substrate can be grouped into three categories as shown in the figure 6.1. Because an inductor's Q is inversely proportional to the series resistance of its metal conductor trace, high conductivity and conductors are desirable.

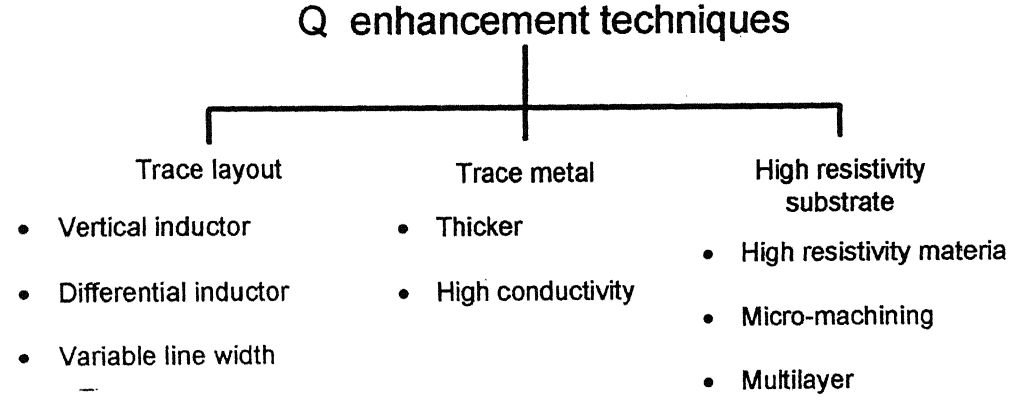

Figure 6.1 Q enhancement Techniques

Other Q-enhancement techniques include using variable line width, the differential excitation technique, and multilayer dielectric and metallization. In the latter case the improvement in Q is achieved by reducing both the dc resistance using thicker

conductors and parasitic capacitance using a multilayer dielectric medium. The Q-factor of a coil can be enhanced by increasing its area and reducing the dc resistance by using a wider line width. However, the parasitic capacitance of the inductor trace and the RF resistance due to eddy currents increase with line width; this sets a maximum limit for the line width.[18]

It has been shown experimentally that the quality factor of spiral inductors can be increased by reducing magnetically induced currents in the trace width by narrowing the line width of the inner turns similar to a silicon micro-machined inductor.

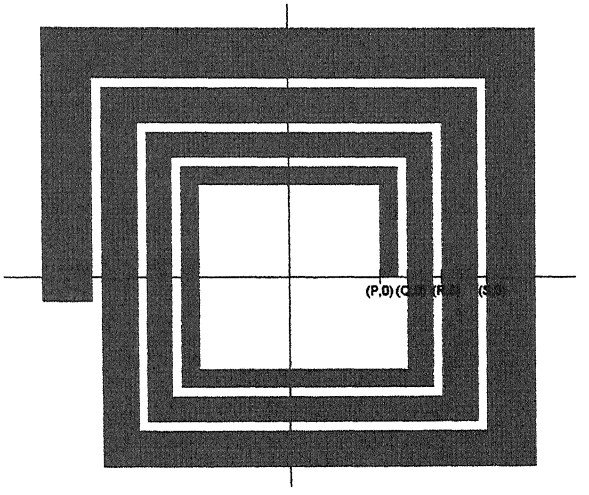

Figure 6.2 Inductor with variable line width

Several square spiral inductors using different line widths and number of segments are designed.

We have varied the variable line width in two different types which are as follows-

- Geometric Progression Variation
- Parabolic Variation

Standard inductors are made of 7, 11 and 15 segments have a constant line width of 20 μm, where as modified inductors are also made 7, 11 and 15 segments have different line widths for each turn depend upon whether it is geometric progression or parabolic variation in the line widths. The variations are varied are discussed as below.

Table 6.1
Quality Factor of Standard Inductors

Standard Inductor	Quality Factor of Inductor at 0.5 f_{res}
7 Segment	40.071
11 Segment	32.522
15 Segment	31.88

6.3.1. Geometric Progression

The figure shows the points (P,0), (Q,0), (R,0) and (S,0). Let W_i be the inner width of the inductor and a be the width of first line, r be the common ratio and s be the separation between the lines then the value of P, Q, R and S are calculated below:

$$P = \frac{W_i}{2}$$

$$Q = \frac{W_i}{2} + a + s$$

$$R = \frac{W_i}{2} + ar + 2s$$

$$S = \frac{W_i}{2} + ar^2 + 3s$$

6.3.2. Parabolic Variation

In the parabolic variation we vary the focal point of the parabola. As shown in figure below as we increase the value of 'a' in $y^2=4ax$ the parabola is extended.

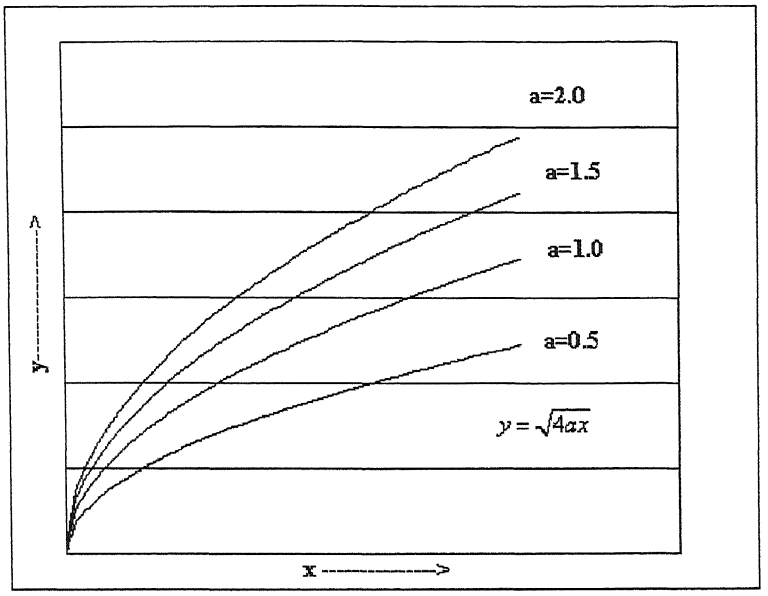

Figure 6.3 Parabolic Variation of line width

The values of P, Q, R and S for the parabolic variation are given as follows

$$P=\frac{W_i}{2}$$

$$Q=\frac{W_i}{2}+s+\sqrt{4a(P+s)}$$

$$R=\frac{W_i}{2}+2s+\sqrt{4a(Q+s)}$$

$$S=\frac{W_i}{2}+3s+\sqrt{4a(R+s)}$$

where W_i is the inner width of the transformer, a is distance between the origin and focal point of the parabola and s is the spacing between adjacent lines. For all the calculation W_i is chosen as 200um and s is 10 um and first width is 20 um.

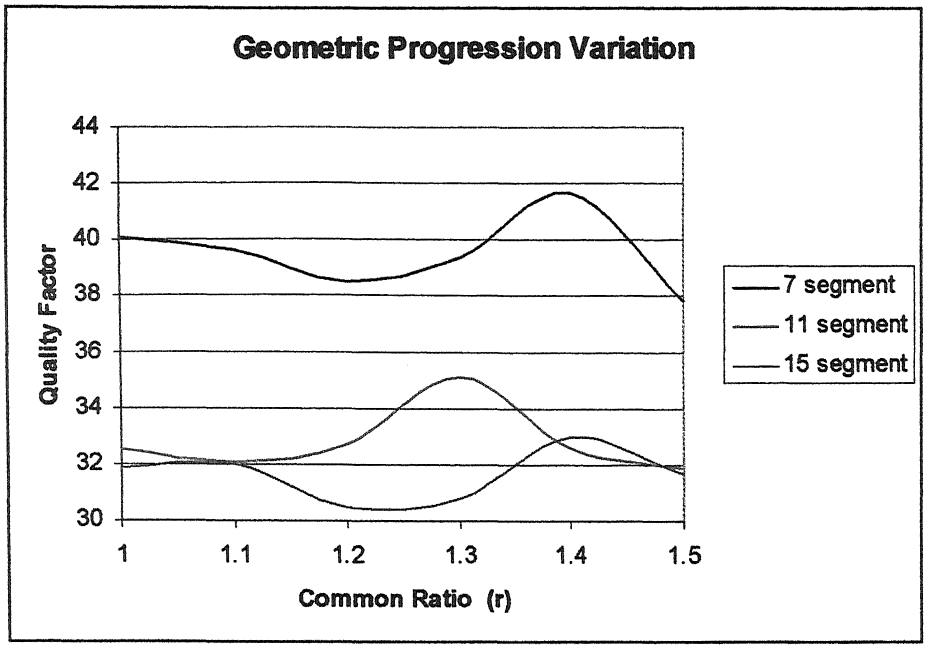

Figure 6.4 Quality Factor vs Common Ratio in Geometric Progression Variation

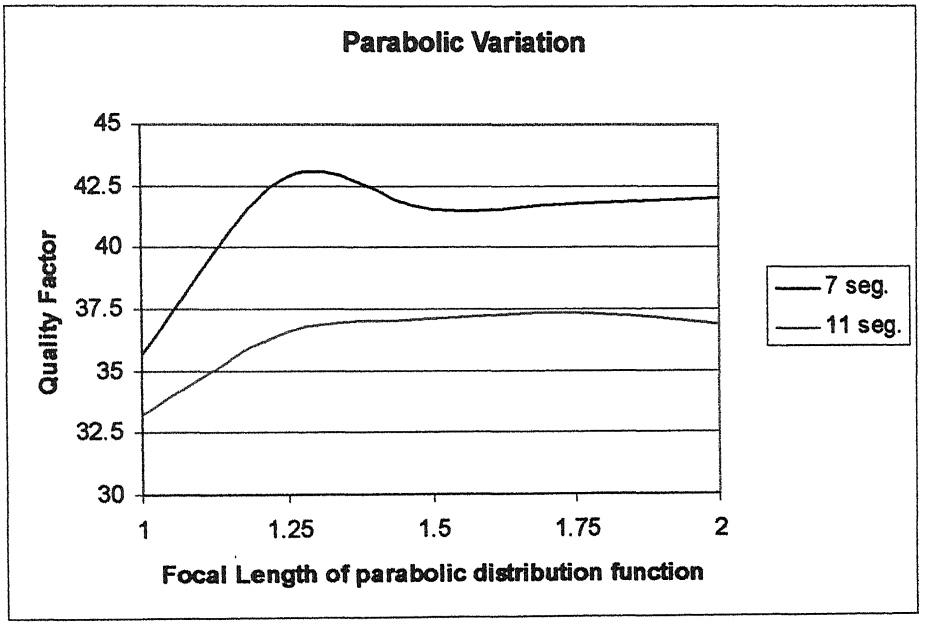

Figure 6.5 Quality Factor vs focal distance of the parabola for 11 segment square inductor

From the figures 6.4 and 6.5 , it is shown that that quality factor of the inductor first increases as increase in common ratio for the geometric progression and focal distance in the parabolic varaition in the line width. and it attains some peak value which is different for each number of segment in geometric variation.

For the similar number of segment in the inductor i.e 11 shown here Q factor is more in the parabolic variation than geometric variation which is better in the circuit applications of inductor more Q reduce the phase noise.As phase noise is inversely proportional square of quality factor which improves the circuit performance.

Chapter 7

Conclusion

7.1 Conclusion

In this work methods have been presented that allow a fast characterization of monolithic integrated inductors and transformers in GaAs technology. The characterization is based on an equivalent electrical low-order model. All parameters of the model are extracted from the physical structure of the device.

We had made some modelling of inductor and transformer for TriQuint GaAs process and compared it with measurements . It shows good results with the inductor but with the transformer it shows good results for lower frequency range. The deviation between the measured and simulated is due to some extra coupling rather than alternate lines and also number of segments is increased in the transformer.

A method for parameter extraction and background details about all elements used in the equivalent-circuit have been presented. The electrical behaviour derived from complex inductors and transformers can be accurately predicted.

7.2 Future Work

In this thesis, we have presented the characterization of the inductor and transformer for TriQuint GaAs process. It shows the good agreement between the measured and simulated results. The better accuracy can be achieved if the coefficients of inductance, substrate capacitance, serial resistance coupling factor and inter-winding capacitance are optimized. An algorithm can be written for the optimization.

For making this characterization of inductors and transformers user friendly, i.e. for inductors or transformers having larger number of segments, we can write macros for the specific design. The macros are the desired sequence of commands which are to be executed to get the specific model. These macros for various designs can be written and stored as library functions for different inductors and transformers.

Appendices

Appendix A

The values of the inductance , capacitance and resistance for a single structure are as follows

Inductance nH

Table A1

W / L		20 um	15 um	10 um	5 um
	ADS	0.691	0.74	0.806	0.906
1000 um	HFSS	0.63	0.681	0.771	0.916
	MOM	0.779	0.852	0.96	1.1970
	ADS	0.523	0.559	0.61	0.686
750 um	HFSS	0.466	0.563	0.6	0.61
	MOM	0.618	0.672	0.755	0.916
	ADS	0.352	0.376	0.41	0.463
500 um	HFSS	0.323	0.378	0.399	0.455
	MOM	0.42	0.458	0.5165	0.633
	ADS	0.178	0.19	0.208	0.236
250 um	HFSS	0.169	0.196	0.203	0.221
	MOM	0.241	0.238	0.271	0.334

Substrate Capacitance pF

Table A2

W / L		20 um	15 um	10 um	5 um
	ADS	0.0385	0.0342	0.029	0.024
1000 um	HFSS	0.044	0.0388	0.0331	0.029
	MOM	0.0377	0.0336	0.0291	0.0317
	ADS	0.029	0.0258	0.02214	0.0182
750 um	HFSS	0.0429	0.0236	0.024	0.015
	MOM	0.0369	0.034	0.031	0.0265
	ADS	0.0174	0.0174	0.0151	0.0127
500 um	HFSS	0.0177	0.0177	0.0162	0.0145
	MOM	0.0237	0.0238	0.0222	0.0212
	ADS	0.01	0.009	0.008	0.007
250 um	HFSS	0.011	0.0108	0.0099	0.0077
	MOM	0.0185	0.135	0.0135	0.0132

Resistance Ohm

Table A3

W		20 um	15 um	10 um	5 um
L					
	ADS	0.9247	1.1431	1.5223	2.4725
1000 um	HFSS	0.3293	1.671	3.05	3.5901
	MOM	1.0231	1.8738	1.8738	3.7406
	ADS	0.6814	0.8436	1.1253	1.8327
750 um	HFSS	0.4573	0.5399	2.4598	2.5485
	MOM	0.7484	1.8738	1.3669	2.6662
	ADS	0.4493	0.5562	0.7423	1.2109
500 um	HFSS	0.1543	1.5293	1.0007	1.9318
	MOM	0.4862	0.6233	0.8874	1.6911
	ADS	0.2232	0.2761	0.3683	0.601
250 um	HFSS	0.2825	0.2692	0.6302	0.5981
	MOM	0.1161	0.3061	0.4347	0.8153

Appendix B

The value of coupling factor and the inter-winding capacitance is given as

Coupling Factor

For length=1000 um

Table B1

Width (um)	20	15	10	5
Spacing (um)				
5	0.638417	0.647731	0.650962	0.66855
10	0.559277	0.566771	0.587893	0.585899
15	0.513958	0.518791	0.528403	0.531142
20	0.479221	0.481844	0.490031	0.490202
30	0.426012	0.42553	0.432332	0.422365
50	0.353745	0.350024	0.353932	0.323287
100	0.246161	0.243378	0.233782	0.201652
200	0.153409	0.156799	0.153516	0.120499
300	0.130231	0.136452	0.134907	0.100377
500	0.120905	0.12853	0.127886	0.092611

For length=750 um

Table B2

Width (um)	20	15	10	5
Spacing (um)				
5	0.664782	0.672375	0.664377	0.685401
10	0.583004	0.593288	0.597525	0.600568
15	0.537715	0.545347	0.546669	0.542962
20	0.502316	0.507707	0.50392	0.494644
30	0.44184	0.442023	0.434459	0.425143
50	0.354267	0.352533	0.345423	0.333753
100	0.240131	0.23863	0.227838	0.214349
200	0.14749	0.14597	0.14139	0.140086
300	0.122288	0.122879	0.120643	0.123033
500	0.112205	0.113821	0.112656	0.123014

For length=500 um

Table B3

Width (um)	20	15	10	5
Spacing (um)				
5	0.69438	0.702964	0.69866	0.702596
10	0.611365	0.621491	0.624234	0.615268
15	0.565109	0.572208	0.562177	0.542885
20	0.520529	0.520522	0.510176	0.490063
30	0.445902	0.444532	0.435634	0.416288
50	0.349856	0.347776	0.341476	0.326322
100	0.224527	0.224307	0.213334	0.220115
200	0.126172	0.138265	0.109023	0.153835
300	0.109575	0.112335	0.0796067	0.138795
500	0.0990584	0.102185	0.0608636	0.133321

For length=250 um

Table B4

Width (um)	20	15	10	5
Spacing (um)				
5	0.771583	0.77491	0.752369	0.746165
10	0.671787	0.68134	0.673372	0.647703
15	0.62333	0.620808	0.588956	0.554476
20	0.557739	0.553449	0.526376	0.498466
30	0.465965	0.462614	0.440272	0.417435
50	0.354281	0.352917	0.330376	0.32188
100	0.212524	0.217248	0.196713	0.210698
200	0.103089	0.103219	0.0873606	0.142439
300	0.0652099	0.0704486	0.0519946	0.126779
500	0.0443192	0.0541944	0.0303306	0.120924

Inter-winding Capacitance

For length= 1000 um

Table B5

Width (um)	20	15	10	5
Spacing (um)				
5	0.0384978	0.0150193	0.0116687	0.00716149
10	0.0103582	0.009012	0.00655811	0.00303961
15	0.0077434	0.0063748	0.00436402	0.00139357
20	0.00563878	0.00479481	0.00308278	0.00046357
30	0.00348563	0.00293967	0.00161324	7.06e-16
50	0.00143102	0.00120072	0.00032268	1.35e-07
100	1.3978e-6	1.12e-07	7.2848e-08	4.11e-15

For length=750 um

Table B6

Width (um)	20	15	10	5
Spacing (um)				
5	0.0122332	0.0106618	0.00839131	0.00535351
10	0.00740495	0.00620325	0.00451292	0.00240905
15	0.00525522	0.00427389	0.00294002	0.00130189
20	0.00395162	0.00313648	0.00208414	0.00079672
30	0.00245753	0.00190311	0.0012036	0.00027603
50	0.0011165	0.0008196	0.00043022	1.35e-07
100	0.00012852	3.38e-05	1.65e-12	3.86e-15

For length =500 um

Table B7

Width (um)	20	15	10	5
Spacing (um)				
5	0.00806773	0.00696651	0.00525486	0.00361379
10	0.00484136	0.00400915	0.00276563	0.00169759
15	0.003427	0.00274611	0.00178765	0.0010895
20	0.00259634	0.00205154	0.00127493	0.00078657
30	0.00165841	0.00128116	0.00072184	0.00047729
50	0.00080877	0.00060321	0.00024907	0.00022182
100	0.00019795	0.00012603	3.58321e-07	3.92e-05

For length =250 um

Table B8

Width (um)	20	15	10	5
Spacing (um)				
5	0.00402293	0.0034105	0.00260088	0.0019042
10	0.00238134	0.00191975	0.00135885	0.00096053
15	0.0016772	0.00129727	0.00087908	0.00068507
20	0.00126809	0.000950889	0.0006229	0.00050189
30	0.00080266	0.000568893	0.00035123	0.00035073
50	0.000386651	0.00023863	0.0001477	0.00023139
100	9.33099E-05	1.17E-05	2.39612E-08	0.00015109

Bibliography

1. E.Pettenpaul et al, " CAD Models of Lumped Elements on GaAs upto 18 GHz,"IEEE Trans. On MTT, vol. MTT-36 , pp. 294-304, Feb. 1988.

2. C.P. Yue and S.S Wong, " On-chip Spiral Inductors with Patterned Ground shields for Si Based RF IC's," IEEE J. Solid State Circuits, vol.33,no.5, May 1998.

3. A.M Niknejad and R.G.Meyer , " Analysis and Optimization of Monolithic Inductors and Transformers for RF ICs," Proc.IEEE Custom Integrated Circuits Conference,pp. 375-378, 1997.

4. Daly, D.A., et al., " Lumped Elements in Microwave Integrated Circuits," IEEE Trans. Microwave Theory Tech., Vol. MTT-15, December 1967, pp. 294-304.

5. Agilent Advanced Design System 2003A, Agilent Technologies Palo Alto, CA 94304.

6. High Frequency Structure Simulator, Ansoft Corporation Inc. pittsburg, PA 15219-1119.

7. MATLAB 6.1 , The Mathworks INC. 2001.

8. J.R Long, "Modeling of Monolithic Inductors and Transformers for Silicon RFIC Design," MTT-S 1995 International Topical Symposium.

9. H. M. Greenhouse , "Design of planar rectangular microelectronic inductors," IEEE trans. Parts, Hybrids, Packaging vol. PHP-10, pp 101-109, June 1974.

10. Zu, L., et al., "High Q-Factor Inductors Integrated on MCM Si Substrates," IEEE Trans. Comps. Packaging Manufacturing Tech. – Part B, Vol. 19, August 1996, pp 635-642.

11. A.W. Lofti and F. C. Lee, " Two-Dimensional Skin Effect in Power Foils for High-Frequency Applications," IEEE Transactions on Magnetics, vol. 31 no. 2, March 1995.

12. Mohan, S.S., et al., " Simple accurate Expressions for Planar Spiral Inductances," IEEEE J. Solid-State Circuits, Vol.34, October 1999, pp. 1419-1424.

13. Y.K.Koutsoyannopoulos, and Yannis Papananos, "Systematic Analysis and Modeling of Integrated Inductors and transformers in RF IC Design," IEEE Trans. On Circuits and Systems –II :Analog and Digital Signal Processing vol. 47, no. 8, pp. 699-713, August 2000.

14. Niknejad, A. M., and R.G. Meyer, " Analysis, Design and Optimization of Spiral Inductors and Transformers for Si RF ICs," IEEE J. Solid State Circuits, Vol. 33 October 1998, pp. 1470-1481.

15. Groves, R., D. L.Harame, and D Jadus, " Temperature Dependence of Q and Inductance in Spiral Inductors Fabricated in a Si-Ge / BiCMOS Technology," IEEE J. of Solid State Circuits, Vol. 32, September 1997, pp. 1455-1459.

16. Zhao ,J et al., "S Parameters-Based Experimental Modeling of High Q MCM Inductor with Exponential Gradient Learning Algorithm," IEEE Trans. Comp. Packing Manu. Tech. Part-B, Vol. 20, August 1997, pp. 202-210.

17. Lutz, R.D., et al., "Modeling and Analysis of Multilevel Spiral Inductors for RFICs," IEEE MTT-S Int. Microwave Symp. Digest., 1999, pp. 43-46.

18. Bahl,I.J., "High Performance Inductors," IEEE Trans. Microwave Theory techniques, Vol. 49, April 2001, pp. 654-664.

19. Matthaei, G.L., L.Young, and E.M.T. Jones ,Microwave Filters, Impedance-Matching Networks and Coupling Structures, New York: McGraw-Hill, 1964, p. 214.

20. Caulton, M., S.P. Knight, and D.A.Daly, "Hybrid Integrated Lumped Element microwave Amplifiers," IEEE Trans. Electron Devices, Vol. ED-15, 1968, pp. 459-466.

21. Wheeler, H.A., "Simple Inductance Formulas for Radio Coils," Proc. IRE, Vol. 16, October 1928, pp. 1398-1400.

22. Zu, L., et al., "High Q-Factor Inductors Integrated on MCM Si Substrates," IEEE Trans. Comps. Packaging Manufacturing Tech. – Part B, Vol. 19, August 1996, pp 635-642.